Stable isotope and Ar-Ar evidence of prolonged multi-scale fluid flow during exhumation of orogenic crust: example from the Mont Blanc and Aar massifs (NW Alps)

Magali Rossi, Yann Rolland

AGU PUBLICATIONS

Tectonics

RESEARCH ARTICLE
10.1002/2013TC003438

Key Points:
- Vein opening as a joint between major shear zones formed at 16 to 12 Ma
- Fluid-rock interaction occurred in an open system at crustal scale
- The vein system remained open to fluid circulation during 4 to 5 Ma

Correspondence to:
Y. Rolland,
yrolland@unice.fr

Citation:
Rossi, M., and Y. Rolland (2014), Stable isotope and Ar/Ar evidence of prolonged multiscale fluid flow during exhumation of orogenic crust: Example from the Mont Blanc and Aar Massifs (NW Alps), *Tectonics*, *33*, 1681–1709, doi:10.1002/2013TC003438.

Received 11 SEP 2013
Accepted 17 JUN 2014
Accepted article online 25 JUN 2014
Published online 12 SEP 2014

Stable isotope and Ar/Ar evidence of prolonged multiscale fluid flow during exhumation of orogenic crust: Example from the Mont Blanc and Aar Massifs (NW Alps)

M. Rossi[1] and Y. Rolland[2]

[1]EDYTEM, Université de Savoie – CNRS, UMR 5204, Le Bourget du Lac, France, [2]Géoazur, UMR 7329, CNRS-UNS-UPMC-IRD, Valbonne, France

Abstract The spatial and temporal scales and the geometry of fluid pathways in a collisional orogen are investigated using stable isotope analysis (O, C, and H) and $^{40}Ar/^{39}Ar$ dating of vein minerals formed at circa 11–16 Ma in the Mont Blanc and the Aar External Crystalline Massifs. In both massifs $^{40}Ar/^{39}Ar$ dating of veins adularia provides evidence for progressive crystallization from 16 to 9 Ma, and mainly at 11–12 Ma following veins opening during shear zone activity. The fluid flow duration thus ranges from 4 to 5 Ma in the two massifs. The $\delta^{18}O$ values of vein quartz and calcite are similar to those of undeformed crystalline and sedimentary host rocks, suggesting rock buffering, while carbon isotope ratios of vein calcites fall into three compositional groups. A-type veins have $\delta^{13}C$ values that are buffered by the Helvetic metasediments, which suggests that these veins formed in a closed system from a locally derived CO_2-rich fluid. The fluid in equilibrium with C-type veins has depleted $\delta^{13}C$ values similar to mantle-CO_2, while the intermediate $\delta^{13}C$ values of B-type veins suggest mixing between the A-type and C-type fluids. These results are in agreement with crustal- to lithosphere-scale upward vertical fluid flow along vertical shear zones related to the strike-slip system bounding the Adriatic block since 16–20 Ma, connecting a deep-seated fluid to some downward flow in the sedimentary cover of External Crystalline Massifs.

1. Introduction

The question of fluid sources and pathways in the crust is a major issue in the field of Earth Sciences regarding, for instance, the processes of ore formation, the rheological behavior of deep parts of seismic faults, or more recently, in stable isotope-based paleo-altimetry [e.g., *Rowley et al.*, 2001]. Stable isotope analysis (O, C, and H) coupled with $^{40}Ar/^{39}Ar$ dating is a powerful approach to examine the duration and architecture of fluid flow percolating through shear zones and veins and the extent of fluid-rock isotope exchange along flow paths [e.g., *Kerrick et al.*, 1978; *McCaig et al.*, 1990; *Mullis et al.*, 1994; *Pili et al.*, 1997; *Valley and Cole*, 2001; *Badertscher et al.*, 2002; *Raimondo et al.*, 2011]. Indeed, as fluid reservoirs have distinct isotope compositions, it is possible to place constraints on fluid sources [*Sheppard*, 1986]. Compositional variations can be interpreted in terms of fluid mixing and isotope exchange between the infiltrated fluid and the host rocks along the fluid pathways [*Kerrick et al.*, 1978, 1980; *Ferry and Dipple*, 1991; *Dipple and Ferry*, 1992; *Dunn and Valley*, 1992; *Ferry and Gerdes*, 1998]. Stable isotopes thus provide key data to explore the scale of fluid redistribution between various fluid reservoirs via networks of active shear zones and associated veins. For instance, the use of stable isotopes is being attempted in vein minerals to decipher mountain ranges paleoaltimetry, based on the hypothesis that fluids retain their meteoric signature [*Rowley et al.*, 2001]. Shear zones are commonly considered as highly permeable fluid pathways when they are active [*Kerrick et al.*, 1978; *Pili et al.*, 1997; *Ferry and Dipple*, 1991; *Dipple and Ferry*, 1992; *Streit and Cox*, 1998]. However, the size, origin, and extent of fluid migration are still a matter of debate. In shear systems, there are indeed evidences of outcrop-scale up to crustal-scale fluid redistribution [e.g., *Kerrick et al.*, 1978, 1980; *Glazner and Bartley*, 1991; *McCaig et al.*, 1990; *Dipple and Ferry*, 1992; *Marquer et al.*, 1994; *Oliver and Bons*, 2001; *Richards et al.*, 2002; *Cartwright and Barnicoat*, 2003, and references therein; *Raimondo et al.*, 2011]. In the External Alps (Figure 1), several studies have examined stable isotopes and fluid inclusions [e.g., *Poty et al.*, 1974; *Marquer and Bukhard*, 1992; *Mullis et al.*, 1994; *Sharp et al.*, 2005] in order to constrain fluid-rock interactions associated with the formation of shear zones at midcrustal depths in the External Crystalline Massifs (ECM) and at upper crustal depth in the Helvetic nappes (sedimentary cover sequence of

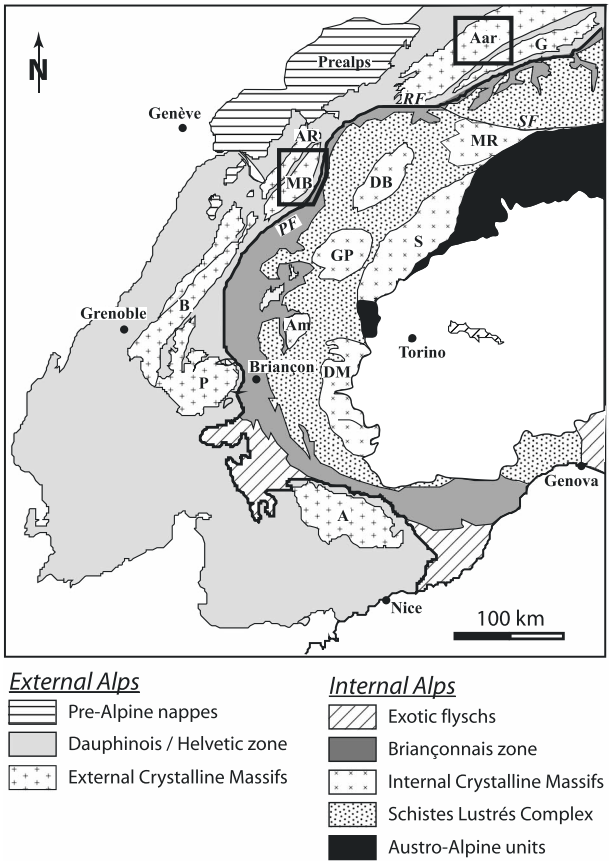

Figure 1. Geological setting of the Western Alps. External crystalline massifs: Aar; G: Gothard; AR: Aiguilles Rouges; MB: Mont Blanc; B: Belledonne; P: Pelvoux; and A: Argentera. Internal crystalline massifs: MR: Monte Rosa; DB: Dent Blanche; GP: Gran Paradiso; S: Sesia; Am: Ambin; DM: Dora Maira. PF: Penninic Front; RF: Rhone Fault; and SF: Simplon Fault. The black squares show the location of the studied area.

the ECM, subjected to nappes stacking during the Alpine orogeny). On the basis of $\delta^{18}O$ distribution in shear zones and neighboring veins, *Fourcade et al.* [1989] and *Marquer and Burkhard* [1992] proposed a two-step tectonic model for the Aar crystalline basement and its metasedimentary cover: (i) fluid circulation in relatively closed systems in minor and weakly deformed shear zones as well as in the alpine veins and (ii) large open-system fluid flow in mylonites and ultramylonites from major shear zones. On the basis of a significant decrease in the $\delta^{13}C$ isotope composition of carbonates toward main thrusts, *Crespo-Blanc et al.* [1995] and *Kirschner et al.* [1999] showed that large-scale fluid circulation occurred in relatively open systems in the Helvetic nappes cover sequence. The decrease of $\delta^{13}C$ isotope compositions observed from the foreland toward the hinterland part of Diablerets and Glarus nappe thrusts (Helvetic nappes translated over the Aar and Gothard Massifs in the Swiss Alps, Figure 1) [*Escher et al.*, 1993] is interpreted either as the result of progressive alteration of the fluid's composition by isotope exchange with carbonates along the fluid pathway or as the effect of fluid dispersion from the main thrust contact [*Baumgartner and Rumble*, 1988; *Burkhard et al.*, 1992; *Crespo-Blanc et al.*, 1995]. Similar decreases in values of $\delta^{18}O$ and $\delta^{13}C$ of veins relative to their wall rocks were found by *Marquer et al.* [1994] and *Kirschner et al.* [1999] in the Aiguilles Rouges Massif and in the Helvetic nappes. Low values of $\delta^{13}C$ were interpreted by *Marquer et al.* [1994] to result from isotope exchange with CO_2 generated by decarbonation of preexisting carbonates. However, *Kirschner et al.* [1999] noted that such decarbonation would not have significantly lowered the $\delta^{18}O$ compositions. Most of the available isotope data from the external Alps are sampled in the Helvetic metasedimentary cover, but very few data exist in the crystalline rocks. Obtaining stable isotope data on vein minerals associated with critical ages for their formation and that of related shear zone deformation in the crystalline basement would contribute to the understanding of structural controls on the development of fluid pathways and on the scale of fluid redistribution in collisional orogens.

In this paper, we report stable isotope and $^{40}Ar/^{39}Ar$ geochronological data from veins formed in the Mont Blanc and the Aar Massifs and in their metasedimentary cover (NW Alps). The main advantage of these massifs is to be essentially composed of chemically homogeneous granite or granodiorite that is affected by the Alpine deformation only [e.g., *Marro*, 1986; *Bussy*, 1990; *Challandes et al.*, 2008; *Rolland et al.*, 2003; *Rossi et al.*, 2005]. Alpine deformation is featured by a network of shear zones and associated veins that formed in the last 20 Ma, but the exact timing of vein formation and related fluid flow with respect to the timing of shear zone activity is still unconstrained. Mineralogical and geochemical changes associated with the shear zones development indicate that parts of the network localized substantial fluid flow [*Poty*, 1969; *Rolland et al.*, 2003; *Rossi et al.*, 2005]. Even though the nature of the Alpine fluids has been investigated using fluid inclusion studies [e.g., *Zimmermann and Poty*, 1970; *Poty et al.*, 1974; *Mullis et al.*, 1994; *Fabre et al.*, 2002], the scales of fluid redistribution within these Alpine structures have not yet been constrained.

Comparison of the results with stable isotope data from the Helvetic metasedimentary cover sequence and other ECM of the Western Alps allows to constrain the nature of the fluid reservoirs. Finally, the integration of the isotope data with the known crustal-scale architecture of the Alpine orogen in the Mont Blanc region, interpreted from the ECORS-CROP profile [e.g., *Tardy et al*., 1990; *Roure et al*., 1996], provides insights to the development of fluid pathways and to the scale of fluid redistribution and fluid-rock interactions during the building of a collisional mountain range.

2. Geological Setting

2.1. General Structure of the NW Alps

The Alpine belt results from closure of Tethys Ocean and collision between African and Eurasian plates. The internal units (Figure 1) form a collisional prism composed of the underthrusted European crustal units, remnants of Tethys Ocean made of Jurassic to Cretaceous rocks, which include relics of the oceanic crust and overlying sediments, and klippes of the overriding African plate. Internal units were metamorphosed at high pressure and low to intermediate temperature during subduction of the Tethys Ocean from the Upper Cretaceous to the Eocene times [*Rubatto et al*., 1999, and references therein] and subduction of the European continental margin during the Eocene [e.g., *Duchêne et al*., 1997, and references therein]. Exhumation of the collisional prism was mainly triggered during the upper Eocene and the Oligocene times [e.g., *Ceriani et al*., 2001; *Simon-Labric et al*., 2009]. The external units (Figure 1) that correspond to the subautochthonous and slightly metamorphosed European margin are dominated by Mesozoic-Cenozoic sediments and their basement rocks (Hercynian crystalline rocks generally referred to as the External Crystalline Massifs or ECM). Overthrusting of the internal units over the external domain occurred by top to the west transport in the Western Alps (Mont Blanc Massif and Dauphinois cover), and top to the northwest transport in the Central Alps (Aar and Gothard Massifs and Helvetic cover), along the Penninic Front during the main phase of Alpine collision (upper Eocene to lower Oligocene) [e.g., *Ceriani et al*., 2001; *Simon-Labric et al*., 2009]. In the sedimentary cover of the External Alps, this shortening phase was expressed by folding and transport of nappes, as the sediments were detached from their crystalline basement and transported westward or northwestward to form the Helvetic nappes (see *Escher et al*. [1993] for a review). During the Miocene and the Pliocene, sustained horizontal tectonic compression resulted in the northwestward propagation of the foreland deformation front and associated molassic basin [*Coward and Dietrich*, 1989; *Schmid and Kissling*, 2000]. During this period, the ECM have been transported to the west in the western Alps, to the northwest in the central Alps, and uplifted by the initiation of a deep ramp-thrust system at the base of the ECM. Reactivation of the Penninic Front thrust system by dextral transpressional faulting occurred in possible connection with the rotation of Apulia [*Rolland et al*., 2012]. As a result, the ECM have truncated the former Helvetic nappe pile resulting in a strongly transpressive "pop-up" structure in the Mont Blanc Massif. The ECM shear zone network connects laterally to the Rhone-Insubric line strike-slip system, and to the southern Aar shear zone domain, where ductile shear zone deformation is documented to occur from 20 to 12 Ma [*Rolland et al*., 2009; *Campani et al*., 2010], while brittle deformation and fluid flow continued until 8–6 Ma [*Berger et al*., 2013] as along the western ECM arc [*Gasquet et al*., 2010].

2.2. Geology of the Mont Blanc Massif

The Mont Blanc Massif (MBM) is an ECM made of polymetamorphic and igneous rocks (Figures 2 and 3). Paragneisses, orthogneisses (dated at 453 ± 3 Ma using U/Pb on zircons) [*Bussy and von Raumer*, 1994], and migmatitic gneisses lay on the west and south sides of the massif. Its central part is made of a calc-alkaline intrusive granite [*Baggio*, 1958; *Bussy*, 1990; *Bonin et al*., 1993; *Bussy and von Raumer*, 1994] dated at 303 ± 3 Ma by U-Pb on zircon [*Bussy and von Raumer*, 1994]. As the Mont Blanc granite was emplaced at the end of the Variscan orogenic cycle, it mainly recorded deformation related to Alpine collision. The intrusive contacts are exposed on both the NW and SE sides and have been locally reactivated by transpressive tectonics during the Alpine orogeny.

In the MBM, the Miocene NW-SE horizontal compression developed an anastomosing network of subvertical shear zones striking N10°E to N40°E that isolates large boudins of weakly strained to unstrained granite (Figure 3). Along a NW-SE transect, this shear zone network has a fan-like arrangement, with NW verging shear zones in the NW and SE verging shear zones in the SE [*Antoine et al*., 1975; *Bertini et al*., 1985; *Bellière*, 1988; *Rossi et al*., 2005]. Inversion of fault and striae data from brittle-ductile shear zones

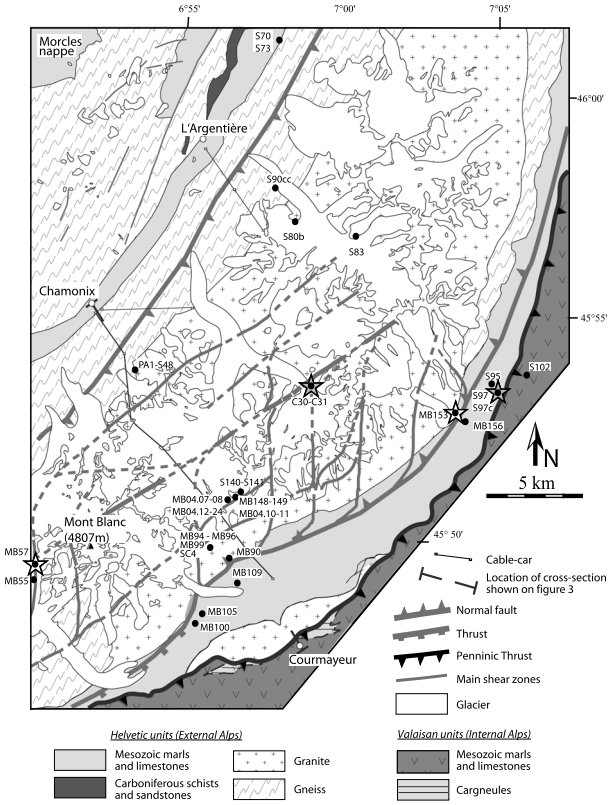

Figure 2. Simplified tectonic map of the Mont Blanc Massif showing sample localities. Main shear zones are reported from aerial photographs. Dashed lines represent interpolation of the shear zone network hidden beneath the glaciers. The stars show the locations of ^{13}C-depleted samples (C-type veins; Figures 9 and 10); samples C31 and S97c are furthermore associated to two metasomatic zones (grey stars). Modified after *Baggio* [1958] and *Bussy* [1990].

indicates horizontal NW-SE shortening [*Rossi et al*., 2005]. These data are in agreement with a model of westward thrusting of the MBM [*Leloup et al*., 2005], at the horse-tail extremity of the transpressive dextral Rhone fault system (RF in Figure 1) [*Hubbard and Mancktelow*, 1992; *Rolland et al*., 2007, 2008, 2009; *Campani et al*., 2010]. Insight of compressional shear zone deformation is constrained by U-Pb ages of synkinematic allanites is of 29 ± 1 Ma in the center of the Mont Blanc [*Cenki-Tok et al*., 2014], which is synchronous to motion of Penninic Front in the Pelvoux range [*Simon-Labric et al*., 2009]. Reactivation of the pristine shear zone structure by transpressional shear zones defining a pop-up structure [e.g., *Rolland et al*., 2007] is constrained by single grain laser $^{40}Ar/^{39}Ar$ dating of shear zone phengites. On the SE side of the MBM dated top to the SE, ductile deformation is at 15.8–16.0 Ma, whereas on the NW side top to the NW deformation is bracketed between 23.4 ± 0.4 and 14.5 ± 0.3 Ma [*Rolland et al*., 2007, 2008]. These ages are similar to the 14.6–18.5 Ma Ar/Ar ages estimated by *Crespo-Blanc et al*. [1995] and *Kirschner et al*. [1996] on white micas within shear zones of the metasedimentary Helvetic nappes (i.e., sedimentary cover of the MBM). The formation of shear zones was associated with the crystallization of greenschist facies metamorphic epidote, chlorite, and white micas, under pressure and temperature conditions of 300–500 MPa and 400–450°C [*Rolland et al*., 2003; *Rossi et al*., 2005].

Within the weakly strained granite, horizontal shortening resulted in opened subhorizontal type-I veins, a few centimeters to tens of centimeter thick, surrounded by hydrothermally altered granite characterized by a high porosity due to quartz and biotite dissolution (Figure 4) [*Poty*, 1969; *Rossi et al*., 2005]. The veins are larger in their

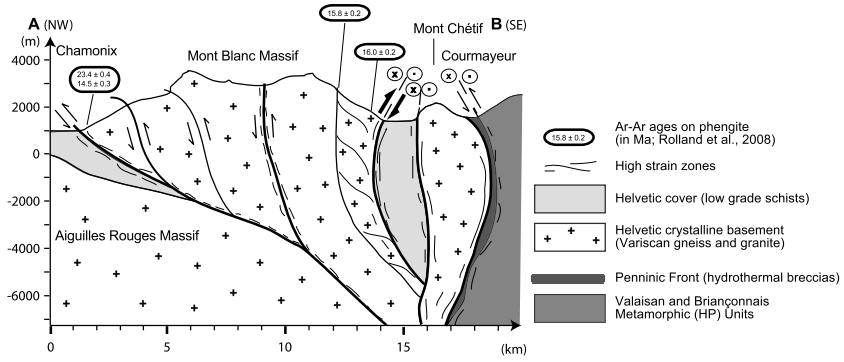

Figure 3. Sketch of a geological cross section across the Mont Blanc Massif, between Chamonix (NW, France) and Courmayer (SE, Italy). The locations of $^{40}Ar/^{39}Ar$ dating performed on phengite from Alpine shear zones are reported (data from *Rolland et al*. [2008]).

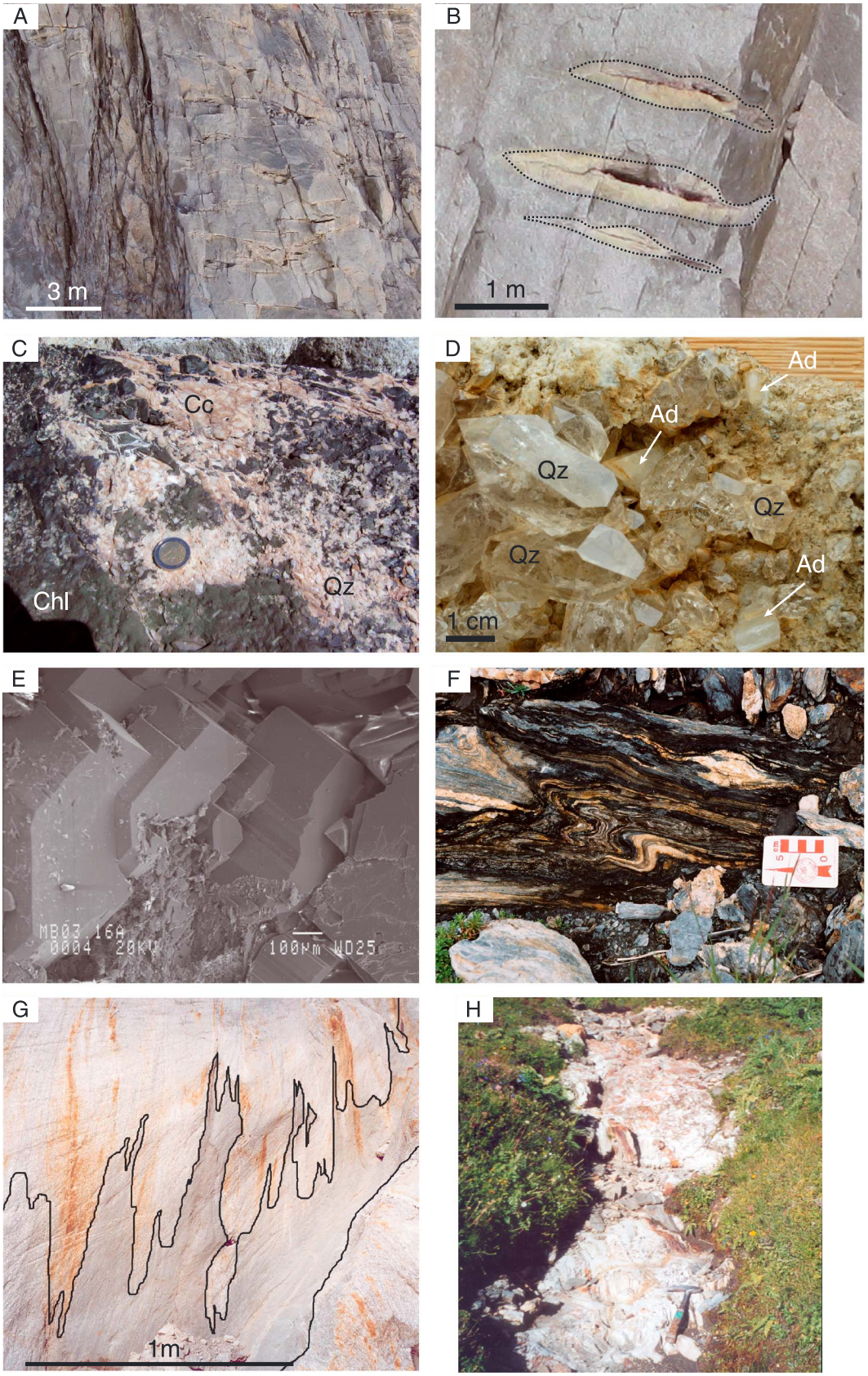

Figure 4

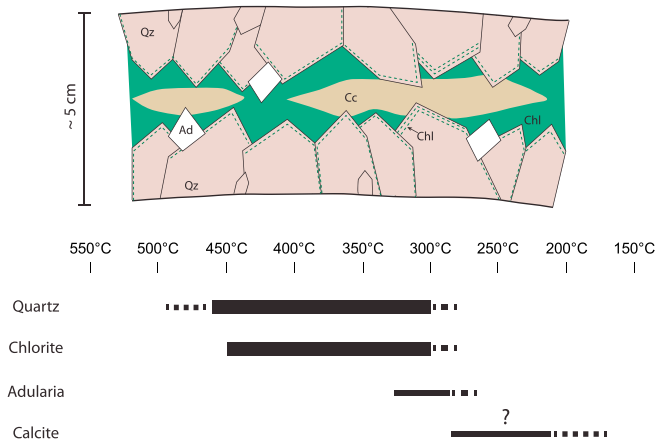

Figure 5. Sketch of a quartz + chlorite ± adularia ± calcite Alpine vein hosted in the external crystalline massifs. The paragenetic sequence is indicated relative to the fluid's temperature, according to stable isotope equilibrium, field observations, and previous studies (see text). The formation temperature of calcite is uncertain but is lower than the other vein minerals. Vein's opening ranges from a few to tens centimeters. Qz = quartz; Chl = chlorite; Ad = adularia; and Cc = calcite.

center and become thinner toward their extremities, where they are usually connected to adjacent shear zones (Figures 4a and 4b). They are mostly filled by a quartz + chlorite ± adularia ± calcite assemblage (Figures 4 and 5) [*Poty*, 1969; *Poty et al*., 1974]. Mineral growth is symmetrical and syntaxial (Figure 5). Quartz grows first, forming abundant and large crystals (from 1 cm to more than 1 dm). In most veins, a thin layer of micrometer-size vermicular chlorite grows together with the last stages of quartz growth; it may develop into a thicker layer covering the quartz ends that sometimes seals the veins. Adularia grows contemporaneously with quartz and chlorite crystals. Calcite is less ubiquitous; it is mainly found on the southeastern side of the massif. When present, it fills the open space after chlorite deposition, thus sealing the veins. In the gneissic basement, the veins analyzed are similar to those described in the granite. Temperatures calculated from fluid inclusions trapped in vein quartz range from 350°C to 420°C [*Poty*, 1969; *Poty et al*., 1974; *Fabre et al*., 2002]. Similar temperatures and pressures of 150–400 MPa were estimated by *Rossi et al*. [2005] for vein chlorites, using the chlorite solid-solution model and thermodynamic data from *Vidal et al*. [2001]. K-Ar dating of vein minerals yields ages of 15.2–18.3 Ma for adularia and 13.4–15.2 Ma for muscovite [*Leutwein et al*., 1970]. Field observations and geochronological data thus suggest that the subhorizontal veins and the subvertical shear zones formed contemporaneously. However, these latter K-Ar dating are dubious due to possible excess and loss of Ar due to hydrothermal processes in alpine shear zone minerals. Only the $^{40}Ar/^{39}Ar$ spectra allow unravel such problems [*Simon-Labric et al*., 2009; *Sanchez et al*., 2011], which will be investigated in this study.

In the center of the MBM, along one of the major shear zones, *Rossi et al*. [2005] described a large metasomatic front (Figures 2 and 4g), which shows upward flow of reactive fluid. These metasomatized rocks are characterized by the replacement of granitic minerals by Mg-rich chlorite and phlogopite [*Rossi*, 2005]. Similar metasomatized rocks were sampled in depth in the center of the massif during digging of the Mont Blanc tunnel. Mass balance calculations performed by *Rossi et al*. [2005] and *Rossi* [2005] on metasomatized samples from the tunnel and the outcrop show huge gains of Mg and Fe (up to 13 wt % Fe_2O_{3T} and 12 wt % MgO), and significant losses of silica and alkali elements (down to 40 wt % SiO_2). Mg enrichment of phyllosilicates observed in some shear zones is interpreted as evidence for the infiltration of the reactive fluid through the connected network of shear zones.

Figure 4. Pictures illustrating the veins and the metasomatic zones sampled for stable isotope analysis. (a) Outcrop illustrating the structural relationships between shear zones (vertical features) and Alpine veins (subhorizontal features) within the MBM. (b) Alpine veins hosted in the weakly deformed granite. Note the alteration halo surrounding the veins (dotted line). (c) Material filling the Alpine veins hosted in the Mont Blanc crystalline rocks. Qz: quartz; Chl: vermicular chlorite; and Cc: calcite. Scale is indicated by the 2 Euro coin. (d) Quartz + adularia vein from the Mont Blanc Massif. Adularia crystals grow contemporaneously with quartz. Qz = quartz and Ad = adularia. (e) Backscattered image of adularia crystals growing in the porosity of the altered Mont Blanc granite surrounding an Alpine vein. (f) Deformed calcite ± quartz veins hosted in the Helvetic metasediments. (g) Metasomatic front (black line) along a vertical granitic wall located in the center of the MBM. Note the vertical digitations showing upward fluid flow along localized vertical "shear" zones, from which pervasive infiltration occurs throughout the granite. Sample C31 was sampled in an Alpine vein close to this metasomatic front. (h) Metasomatic zone from the Mont Blanc sedimentary cover cropping out in a stream bed along the Penninic Front. The white material is made of talc + oxides and the ochre material is made of ankerite + oxides. Sample S97c was sampled in the vicinity of these metasomatized rocks.

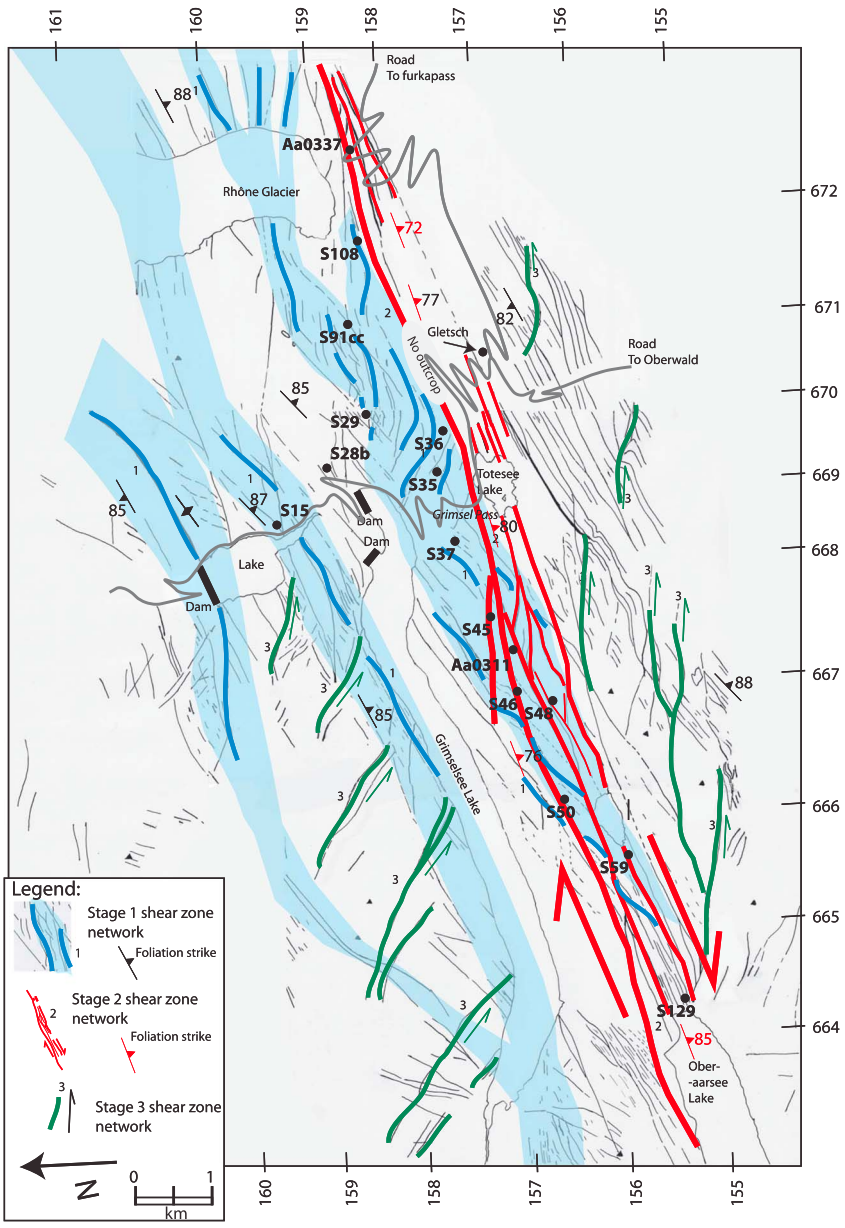

Figure 6. Simplified tectonic map of the Southern Aar Massif (modified from *Rolland et al*. [2009]) showing the several generations of shear zones. Location of sampled veins for Ar/Ar and stable isotope analyses is indicated.

2.3. Geology of the Aar Massif

The geology of the Aar Massif and related shear zone deformation is extensively described in *Rolland et al*. [2009] (Figures 1 and 6). Main features are summarized below.

Three sets of steeply dipping shear zones crosscutting the Grimsel granodiorite of the Aar Massif have been identified in the Grimsel Pass area and dated by $^{40}Ar/^{39}Ar$ dating of synkinematic white mica (phengite) and biotite. Stage 1 shear zones (~21 Ma) are very broad (~200 m wide), with a progressive increase in ductile deformation from rim to core, and have a dip-slip kinematics. Similar, though more complex $^{40}Ar/^{39}Ar$ datings were obtained by *Challandes et al*. [2008]. Stage 2 shear zones (15.5–12.2 Ma) are narrower and show a gradual change from dextral strike-slip to dip-slip kinematics along strike. These coincide with Rb-Sr dates of 10–12 Ma. Brittle precursors (~15.5 Ma) of shear zones marked by biotite-rich cataclasites are preserved along the northern contact of the main stage 2 shear zone. These brittle faults localized fluid flow for ~ 2 Ma. Subsequent ductile shear and fluid-induced reaction weakening produced phengite-rich mylonites and

phyllonites. The main event of fluid flow is connected to this stage 2 phase, with alpine veins developing obliquely (10–35°) to the shear zones, in agreement with their transpressional character. These veins show the same quartz + chlorite ± adularia ± calcite assemblage and alteration halo as in the MBM [*Mullis et al*., 1994; *Mullis*, 1996]. Stage 3 shear zones are brittle sinistral strike-slip faults, developing cataclasites, breccias, and clay fault gouges. Previous studies established that these late faults formed at < 9 Ma and were active until at least 3 Ma [*Kralik et al*., 1992]. *Challandes et al*. [2008] estimated maximum burial conditions of 600 ± 100 MPa (20 km) were achieved at 450 ± 30°C. At this temperature, *Goncalves et al*. [2012, 2013] estimated pressure of 650 ± 100 MPa from P-T sections of the protolith, the mylonite, the ultramylonite, and the chlorite-bearing ultramylonite compositions in the NaCaFMASH system under saturated conditions. Therefore, thermobarometric estimates from mineral assemblages in the Aar shear zones range from 300 MPa to 400°C in the north of the massif to 650 ± 100 MPa to 475 ± 25°C in the study area [*Steck and Burri*, 1971; *Steck*, 1976; *Berntat and Bambauer*, 1982; *Frey*, 1987, 1988; *Frey et al*., 1980, 1999; *Frey and Mählmann Ferreiro*, 1999; *Challandes et al*., 2008; *Goncalves et al*., 2012, 2013]. Previous studies concluded that the shear zones formed close to peak metamorphic conditions [*Fourcade et al*., 1989; *Challandes*, 2001; *Challandes et al*., 2008; *Goncalves et al*., 2012, 2013]. Fluid circulation in the shear zone network is indicated by δ^{18}O values in shear zones being up to 2‰ higher in shear zones than in undeformed zones [*Fourcade et al*., 1989]. Fluid-rock interaction during shear zone formation also led to enrichment in K, Mg, and Rb, and depletion in Na, Ca, and Sr [*Marquer et al*., 1985; *Marquer and Peucat*, 1994; *Goncalves et al*., 2012, 2013]. This is consistent with the stability of micas and destabilization of plagioclase during deformation.

2.4. Geology of the Sedimentary Cover of Crystalline Massifs

The sedimentary cover of the Mont Blanc and Aar ECMs crops out along a narrow stripe trapped between the Aiguilles Rouges and the Mont Blanc Massifs on the NW and along a large band that is separated from the internal units on the SE by the Penninic Front, to the SE of the Mont Blanc. Further east, the relationships of the Aar Massif with its sedimentary cover is complexified by strong transpressional deformation along the Rhone valley fault, so the basement-cover relationships are best analyzed in the MBM. On both sides of the MBM, the sedimentary pile is similar and made of Jurassic shales, marls, and limestone (Figures 2 and 3). During the Alpine collision, the sedimentary pile was metamorphosed into the greenschist facies, as for the crystalline basement.

The Morcles nappe, which is the basal nappe of the Helvetic units, was rooted to the southwestern side of the MBM before overlying the Aiguilles Rouges Massif toward the northwest [*Escher et al*., 1993, and references therein]. In the central Swiss Alps, the same structure is called the Doldenhorn nappe. The Ardon and Diablerets nappes are higher Helvetic nappes that were respectively rooted on top and on the southeastern flank of the MBM [*Escher et al*., 1993]. As most Helvetic nappes are rooted in the Mont Blanc sedimentary cover, comparison of stable isotope data from the Helvetic nappes appears relevant.

Along the Penninic Front (i.e., the thrust contact that separates the External Units from the high-pressure Internal Units, Figure 1), a complex zone is developed, which includes lenses of argillite and ankeritic dolomite trapped in a talc matrix. This complex zone is interpreted as remnants of Triassic evaporites transported during thrusting of the Penninic Front that were transformed by hydrothermal fluid-rock interaction (Figure 4h) [*Antoine et al*., 1975]. The reactive fluid may thus have infiltrated the sediments by flowing along the Penninic Front thrust.

Most veins hosted in the sedimentary rocks were sampled from the Mont Blanc Helvetic sediments. They are ptseveral millimeters to a few centimeters thick and are filled by a calcite ± quartz assemblage, with no occurrence of chlorite or adularia (Figure 4d).

3. Methodology and Analytical Techniques

3.1. Stable Isotopic Analysis

For this study, 55 synkinematic veins were sampled for quartz, chlorite, and calcite to perform oxygen, carbon, and hydrogen isotope analysis: 24 veins were sampled in the Mont Blanc granite, 3 veins in the Mont Blanc gneisses, 11 veins in its Helvetic sedimentary cover, 1 vein in the Valaisan unit (S102), and 16 veins in the Grimsel granodiorite (Table 1). Mineral separates with grain diameters of 0.1–1 mm were obtained by handpicking from crushed vein samples.

Table 1. Description of the Host Rock and the Vein Mineralogy

Mont Blanc Massif	Host Rock	Distance From Contact[a] (km)	Vein Mineralogy	Vein Type[b]	Aar Massif	Host Rock	Vein Mineralogy	Vein Type[b]
			Veins					
S70	Helvetic sediments	−0.3	Qz-Cc	A	S11	Granodiorite	Qz	-
S73	Helvetic sediments	−0.1	Qz-Cc	A	S 15	Granodiorite	Qz-Chl	-
S90 CC	Gneiss	0.0	Cc	B	S 28b	Granodiorite	Qz-Cc-Chl	B
PA 1	Granite	1.5	Qz	B	S29	Granodiorite	Qz-Chl	-
S80b	Granite	1.7	Qz-Cc-Chl	B	S35	Granodiorite	Qz-Chl	-
MB 55	Gneiss	3.3	Qz-Chl	B	S 36	Granodiorite	Qz-Cc	C
MB 57	Gneiss	3.5	Qz-Cc-Chl	C	S37	Granodiorite	Qz	-
C 30	Granite	5.5	Chl	B	S45	Granodiorite	Qz-Cc	C
C 31	Granite	5.6	Qz-Cc-Chl	C	S 46	Granodiorite	Qz-Cc-Chl	C
S83	Granite	7.0	Qz-Cc-Chl	B	S48	Granodiorite	Qz-Chl	-
MB04 07	Granite	7.2	Qz-Cc-Chl	B	S48b	Granodiorite	Qz-Chl	-
MB04 08	Granite	7.3	Cc-Chl	B	S50	Granodiorite	Qz-Chl	-
MB 148	Granite	7.4	Chl	B	S 59	Granodiorite	Qz	-
MB04 10	Granite	7.4	Qz-Cc-Chl	B	S91 CC	Granodiorite	Cc	B
MB 149	Granite	7.5	Qz-Chl	B	S 108	Granodiorite	Qz-Chl	-
MB04 11	Granite	7.5	Qz-Cc-Chl	B	S129	Granodiorite	Qz	-
S141 CC	Granite	7.5	Cc	B				
MB04 12	Granite	7.6	Qz-Cc-Chl	B				
MB04 13	Granite	7.7	Cc	B				
MB04 14	Granite	7.8	Cc-Chl	B				
MB04 16	Granite	7.9	Qz-Cc	B				
S140	Granite	8.0	Qz-Cc	B				
MB04 22	Granite	8.1	Qz-Cc-Chl	B				
MB04 24	Granite	8.5	Qz-Cc-Chl	B				
SC 4	Granite	9.2	Qz-Cc	B				
MB 94	Granite	9.2	Chl	B				
MB 96	Granite	9.3	Chl	B				
MB 99	Granite	9.4	Qz-Cc	B				
MB 90	Granite	9.5	Qz-Chl	B				
MB 153	Helvetic sediments	11.0	Qz-Cc	C				
MB 100	Helvetic sediments	11.5	Qz-Cc	A				
MB 156	Helvetic sediments	12.0	Qz-Cc	A				
MB 105	Helvetic sediments	12.5	Qz-Cc	A				
MB 109	Helvetic sediments	13.0	Qz-Cc	A				
S95	Helvetic sediments	13.0	Qz-Cc	A				
S97c	Helvetic sediments	14.0	Qz-Cc	C				
S 97	Helvetic sediments	14.0	Qz-Cc	A				
S 99	Helvetic sediments	14.5	Qz-Cc	A				
S 102	Valaisan sediments	15.0	Qz-Cc	A				

[a]Distance from the contact of the Helvetic sediments and the gneiss on the west side of the MBM. Qz: Quartz; Cc: Calcite; and Chl: Chlorite.
[b]Vein types defined from Figures 5 and 6.

The stable isotope analyses of calcite were performed at the Research School of Earth Sciences (RSES, ANU), Australia. Calcite samples were reacted with H_3PO_4 in a Kiel microcarbonate preparation device at 90°C [*McCrea*, 1950]. The evolved CO_2 gas was measured in a Finnigan MAT 251 mass spectrometer. The $\delta^{13}C$ and $\delta^{18}O$ values of calcite were calibrated relative to NBS-19 (accepted values $\delta^{18}O_{PDB} = 2.20‰$ and $\delta^{13}C_{PDB} = +1.95‰$) [*International Atomic Energy Agency* (*IAEA) catalogue*, 1998]. The long-term measurement precision for NBS-19 at RSES is 0.07‰ (2σ) for $\delta^{18}O$ and 0.04‰ (2σ) for $\delta^{13}C$. Average NBS-19 standard values obtained during measurements were $\delta^{18}O = 2.20 \pm 0.03‰$ and $\delta^{13}C_{PDB} = 1.95 \pm 0.01‰$ ($N = 9$). The average standard error on duplicate samples was 0.02‰. In this paper, the values of $\delta^{18}O$ of calcite are reported relative to Vienna SMOW (VSMOW) ($\delta^{18}O_{PDB} = 1.03091 \times \delta^{18}O_{VSMOW} + 30.91$) [*Coplen et al.*, 1983].

Stable isotope compositions of silicates were analyzed at the Institute of Geological and Nuclear Sciences of Lower Hutt, New Zealand. Hydrogen isotope values of chlorite were determined using the method of *Vennemann and O'Neil* [1993]. Adsorbed water was removed from samples by heating to 200°C in a vacuum for at least 12 h. Water was extracted for hydrogen isotope measurement by heating to temperatures of

Table 2. Summarized $^{40}Ar/^{39}Ar$ Dating Results[a]

Step No.	Laser Power (mW)	^{36}Ar	^{37}Ar	^{38}Ar	^{39}Ar	$^{40}Ar^*$	Age ± 2σ(Ma)	$^{40}Ar^*$(%)	^{39}Ar(k)(%)	K/Ca
					Aar veins					
Sample AA03-11, plateau age: 12.63 ± 1.55 Ma, MSWD: 5.8 (89% ^{39}Ar), isochron age: 14.04 ± 1.18 Ma, MSWD: 0.81 (J = 0.00349845 ± 0.00001749)										
K317-1	550	0.000586	0.11009	0.012119	0.044158	1.228154	167.52 ± 4.22	87.45	4.37	1.97
K317-2	615	0.000117	0.04867	0.002369	0.026251	0.011731	2.82 ± 8.79	24.68	2.60	5.51
K317-3	652	0.000105	0.04458	0.001987	0.042967	0.045242	6.63 ± 3.73	58.19	4.25	10.83
K317-4	705	0.000102	0.05123	0.002624	0.079574	0.113903	9.01 ± 1.08	77.68	7.87	15.41
K317-5	750	0.000063	0.04929	0.002430	0.111114	0.190801	10.81 ± 1.12	89.66	10.99	23.13
K317-6	763	0.000027	0.01552	0.000241	0.122438	0.237177	12.18 ± 0.89	101.84	12.11	-
K317-7	840	0.000058	0.03788	0.001435	0.088410	0.151569	10.79 ± 1.02	88.43	8.75	32.82
K317-8	902	0.000036	0.02243	0.000503	0.151488	0.349096	14.49 ± 0.59	95.80	14.98	-
K317-9	950	0.000045	0.03355	0.001126	0.081082	0.205948	15.96 ± 0.99	92.88	8.02	39.56
K317-10	970	0.000002	0.00000	0.000000	0.040151	0.090092	14.11 ± 2.27	98.12	3.97	-
K317-11	1111	0.000193	0.06816	0.004646	0.223314	0.408679	11.51 ± 0.73	86.39	22.09	24.76
Sample AA03-37, plateau age: 11.51 ± 0.42 Ma, MSWD: 0.17 (81% ^{39}Ar), isochron age: 12.13 ± 0.39 Ma, MSWD: 0.99 (J = 0.00349980 ± 0.00001750)										
K314-1	20	0.000075	0.30983	0.001873	0.000114	0.108543	-	82.88	0.01	0.03
K314-2	615	0.000125	0.44971	0.002676	0.014607	0.007360	-	16.30	1.88	2.76
K314-3	615	0.000174	0.76635	0.004564	0.132946	0.195179	9.25 ± 1.58	77.71	17.08	14.75
K314-4	652	0.000081	0.44094	0.002680	0.101339	0.182611	11.34 ± 1.62	87.00	13.02	19.54
K314-5	700	0.000060	0.38595	0.002377	0.173835	0.330632	11.97 ± 0.82	93.44	22.33	38.28
K314-6	720	0.000081	0.36889	0.002231	0.082622	0.142910	10.89 ± 1.75	84.28	10.61	19.04
K314-7	1200	0.000104	0.57593	0.003487	0.272976	0.494331	11.40 ± 0.52	92.66	35.07	40.29
					Mont Blanc veins					
Sample MB03-70_grain 1, plateau age: 12.5 ± 0.3 Ma, MSWD: 11.4 (92.3% ^{39}Ar), isochron age: 11.3 ± 0.7 Ma, MSWD: 2.74 (J = 0.00349912 ± 0.000017)										
K313-1	605	0.001583	0.13393	0.017937	0.259518	3.129307	74.56 ± 0.86	86.69	7.74	8.02
K313-2	629	0.000014	0.03363	0.001131	0.150213	0.269849	11.30 ± 0.53	96.90	4.48	70.49
K313-3	660	0.000081	0.05844	0.003415	0.332032	0.588120	11.15 ± 0.22	94.54	9.90	51.19
K313-4	680	0.000131	0.06556	0.004297	0.234811	0.472040	12.65 ± 0.58	91.09	7.00	28.31
K313-5	709	0.000680	0.08687	0.007547	0.523773	1.059285	12.72 ± 0.30	82.90	15.61	36.34
K313-6	738	0.000613	0.09043	0.008178	0.613098	1.267755	13.01 ± 0.26	86.30	18.28	39.36
K313-7	772	0.000211	0.07906	0.006250	0.419678	0.878846	13.17 ± 0.23	92.08	12.51	35.53
K313-8	800	0.000012	0.00000	0.000000	0.017469	0.040544	14.59 ± 4.87	108.11	0.52	50.35
K313-9	915	0.000134	0.06793	0.004615	0.291701	0.675395	14.56 ± 0.36	93.29	8.70	33.46
K313-10	1200	0.000165	0.08157	0.006654	0.512074	1.002527	12.32 ± 0.23	93.97	15.27	39.99
Sample MB03-70_grain 2, plateau age: 13.07 ± 0.8 Ma, MSWD: 13 (95% ^{39}Ar), isochron age: 12.8 ± 0.8 Ma, MSWD:3.03 (J = 0.0034645 ± 0.000019)										
K314-1	605	4.717000	0.17029	0.029000	0.207615	26.552000	150.80 ± 2.48	94.69	3.06	6.42
K314-2	629	0.000000	0.11402	0.013000	0.120171	1.999000	12.36 ± 0.34	99.22	6.07	56.39
K314-3	660	0.070000	0.10954	0.012000	0.265625	1.898000	11.61 ± 0.21	98.09	25.71	40.95
K314-4	700	0.036000	0.10954	0.012000	0.187849	2.275000	14.01 ± 0.14	98.84	62.20	22.65
K314-5	800	0.356000	0.10488	0.011000	0.419018	2.229000	13.14 ± 0.28	94.58	75.55	29.07
K314-6	920	0.076000	0.11402	0.013000	0.490478	2.107000	12.89 ± 0.27	98.19	90.06	31.49
K314-7	1200	0.000000	0.10954	0.012000	0.335742	2.077000	12.84 ± 0.12	99.25	100.00	28.43
Sample MB08-22_grain 1, plateau age: 11.41 ± 0.20 Ma, MSWD: 2.5 (16% ^{39}Ar), isochron age: 11.43 ± 0.53 Ma, MSWD: 0.03 (0.00411020 ± 0.000041)										
K604-1	451	0.000168	0.05622	0.003161	0.084549	2.864771	235.22 ± 2.37	98.21	4.09	4402
K604-2	500	0.000003	0.00332	0.000011	0.004318	0.008540	14.61 ± 2.52	111.30	0.21	6978
K604-3	550	0.000001	0.00407	0.000017	0.027404	0.039676	10.70 ± 0.34	98.93	1.32	12116
K604-4	600	0.000000	0.00692	0.000048	0.137418	0.212618	11.44 ± 0.16	98.10	6.64	60271
K604-5	640	0.000004	0.01008	0.000102	0.159366	0.248840	11.54 ± 0.16	97.72	7.70	69048
K604-6	655	0.000017	0.01177	0.000139	0.124069	0.226977	13.51 ± 0.19	96.29	6.00	23323
K604-7	680	0.000011	0.01672	0.000279	0.241774	0.537340	16.41 ± 0.19	98.12	11.68	60508
K604-8	700	0.000024	0.01400	0.000196	0.158472	0.330444	15.40 ± 0.19	96.58	7.66	64769
K604-9	850	0.000024	0.03100	0.000961	1.131921	2.124916	13.87 ± 0.17	98.12	54.70	72454
Sample MB08-22_grain 1, plateau age: –, isochron age: 11.35 ± 0.37 Ma, MSWD: 0.2 (J = 0.00408530 ± 0.00002043)										
K605-1	451	0.000137	0.03230	0.001043	0.002286	0.731362	-	94.73	0.09	245
K605-2	504	0.000008	0.00463	0.000021	0.018076	0.037465	15.21 ± 1.46	93.06	0.70	43705
K605-3	552	0.000001	0.00539	0.000029	0.051980	0.083032	11.73 ± 0.44	98.65	2.00	26373
K605-4	600	0.000007	0.00591	0.000035	0.131688	0.200830	11.21 ± 0.27	99.05	5.07	31260

Table 2. (continued)

Step No.	Laser Power (mW)	^{36}Ar	^{37}Ar	^{38}Ar	^{39}Ar	^{40}Ar*	Age ± 2σ(Ma)	^{40}Ar*(%)	^{39}Ar(k)(%)	K/Ca
K605-5	630	0.000002	0.01084	0.000117	0.208714	0.308057	10.85 ± 0.22	98.24	8.04	89664
K605-6	655	0.000010	0.00684	0.000047	0.145006	0.213573	10.82 ± 0.23	99.44	5.59	40455
K605-7	675	0.000009	0.00826	0.000068	0.199974	0.289940	10.65 ± 0.20	98.89	7.70	224528
K605-8	692	0.000001	0.00926	0.000086	0.162849	0.249512	11.26 ± 0.17	97.99	6.27	105589
K605-9	715	0.000031	0.01338	0.000179	0.203485	0.345268	12.46 ± 0.19	95.80	7.84	69502
K605-10	730	0.000040	0.02029	0.000412	0.257283	0.438085	12.51 ± 0.19	95.73	9.91	103652
K605-11	745	0.000001	0.01068	0.000114	0.099951	0.162394	11.94 ± 0.28	97.97	3.85	48544
K605-12	1111	0.000081	0.02811	0.000790	1.114115	1.791581	11.81 ± 0.14	96.92	42.93	112264

[a]Units in the different Ar isotopes are given in volts.

about 1300°C until volatile release ceased. Hydrogen was reduced with a Zn reagent. Isotope values are reported relative to VSMOW. The reproducibility of δD is usually better than 3‰. Sample values were normalized to an in-house kaolinite standard which has an accepted value of −57‰ (VSMOW). Replicate analyses of this standard were better than 2‰ (2σ, $N = 8$). NBS-30, an international biotite standard was analyzed as a check and an average value of −64 ± 3‰ ($N = 5$) was obtained (accepted value δD = −65.7‰) [*Coplen et al*., 1983; *IAEA catalogue*, 1998].

Oxygen was extracted from silicates using a CO_2-laser and BrF_5 reagent [*Sharp*, 1990]. Samples were normalized to the international quartz standard NBS-28 [*Friedman and Gleason*, 1973]. The in-house measured value is $\delta^{18}O_{VSMOW} = 9.6 \pm 0.2$‰ ($N = 4$; accepted value $\delta^{18}O_{VSMOW} = 9.60$‰). The garnet standard UWG-2 was run as an in-house check standard and values of +5.7 and 5.8‰ were obtained (accepted value is +5.8‰) [*Valley et al*., 1995]. Biotite and chlorite (plus standards) were heated to 200°C prior to loading into the vacuum extraction line to remove adsorbed water. Samples were then pumped out for approximately 12 h. Oxygen yields were recorded and oxygen converted to CO_2 was analyzed on a Geo20-20 mass spectrometer.

3.2. ^{40}Ar/^{39}Ar Dating

Vein adularia was sampled by handpicking under binocular microscope from the selected vein samples (locations are shown on Figures 2 and 6). Samples were then irradiated in the nuclear reactor at McMaster University (Hamilton, Canada), in position 5c, along with Hb3gr hornblende as a neutron fluence monitor, for which an age of 1072 Ma is adopted [*Turner et al*., 1971]. The total neutron flux density during irradiation was 9.0×10^{18} neutron cm^{-2}. The estimated error on the corresponding ^{40}Ar*/^{39}Ar$_K$ ratio is ± 0.2% (1σ). Adularias were analyzed by ^{40}Ar/^{39}Ar using a laser to induce stepwise Ar release. Results are presented in Table 2. Analyses of individual adularia grains (~0.5 mg on average) were made by step heating with a 50 W CO_2 Synrad 48–5 continuous laser beam. Measurement of isotopic ratios was done with a VG3600 mass spectrometer, equipped with a Daly detector system. Detailed procedures are given in *Jourdan et al*. [2004]. Typical blank values for extraction and purification of the laser system are in the range 4.2–8.75, 1.2–3.9, and 2–6 cc STP for masses 40, 39, and 36, respectively.

All measurements were undertaken at the University of Nice (Géoazur, France). The mass discrimination was monitored by regularly analyzing air pipette volume. Decay constants are those of *Steiger and Jäger* [1977]. Uncertainties on apparent ages are given at the 1σ level and do not include the error on the ^{40}Ar*/^{39}Ar$_k$ ratio of the monitor.

4. Results of Ar/Ar Dating of Vein Adularia

Ar spectra resulting from ^{40}Ar/^{39}Ar dating performed on two samples of the Mont Blanc veins (MB08-22 and MB03-70) are shown in Figure 7; those of the Aar veins (AA03-11 and AA03-37) are reported in Figure 8. For each sampled vein of the Mont Blanc Massif, two adularia crystals were dated (*grain 1* and *grain 2*). All spectra show a similar shape with more or less amplification, which includes (i) a first step displaying some excess Ar, which is ascribed to degassing of a low-temperature phase or fluid inclusions; (ii) a low-temperature part with younger ages; and (iii) increasing ages in a "staircase" shape until a maximum age is reached before the last (fusion) step. This shape can be interpreted as core to rim zoning due to progressive growth of vein adularia toward the core of veins (e.g., Figures 4e and 5). In general, inverse isochron correlation does not show sufficient spread in ^{39}Ar/^{40}Ar to be reliable and is not considered in this study, while the isochron plots show sufficient spread for comparisons with the plateau ages, also allowing comparison of samples with each other.

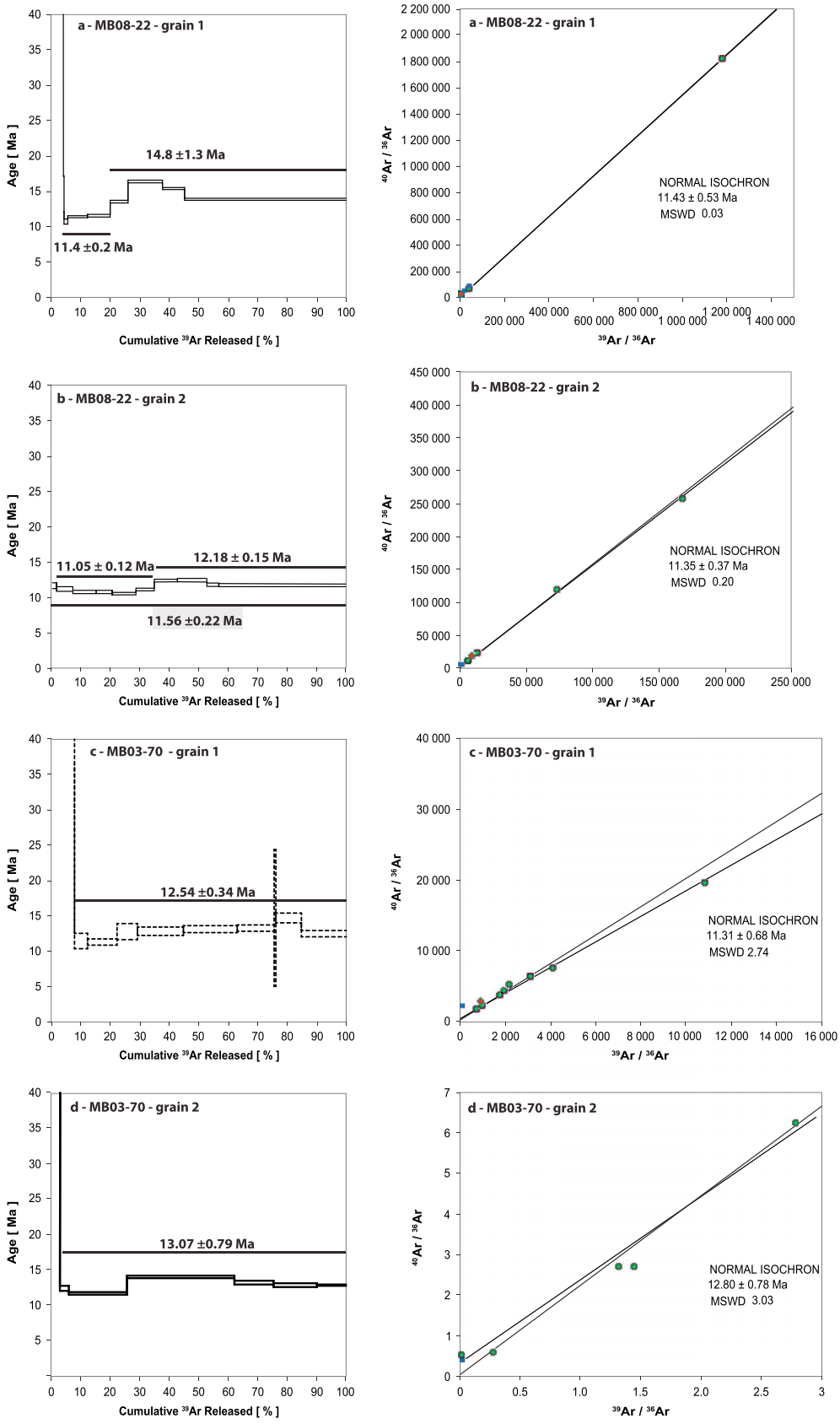

Figure 7. (a–d) Adularia $^{40}Ar/^{39}Ar$ dating results in veins of the Mont Blanc Massif.

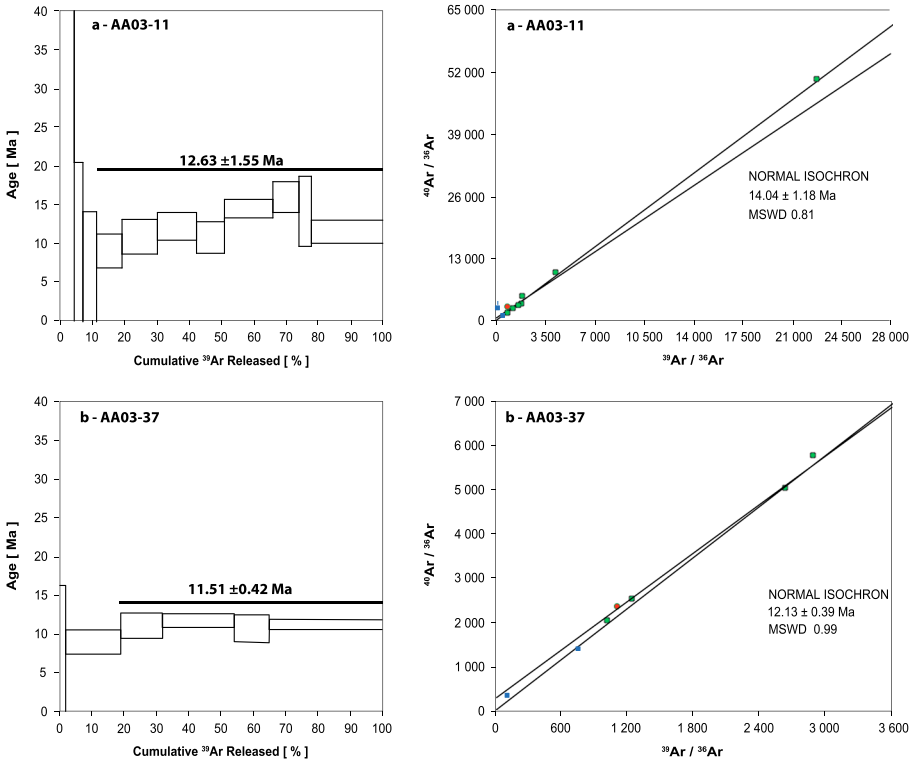

Figure 8. (a, b) Adularia $^{40}Ar/^{39}Ar$ dating results in veins of the Aar Massif.

4.1. Mont Blanc Massif

4.1.1. Sample MB08-22

Sample MB08-22_*grain 1* (Figure 7a) shows no plateau age but a two-part Ar spectrum: (i) steps 2–4 give an age of 11.4 ± 0.2 Ma and (ii) steps 5–8 give an age of 14.8 ± 1.3 Ma. For the low-temperature part, the isochron age is in agreement with the plateau age of steps 2–4 (11.4 ± 0.5 Ma using steps 2–4, mean square weighted deviation (MSWD) = 0.03). Sample MB08-22_*grain 2* shows a plateau age of 11.56 ± 0.22 Ma using all steps except step 1 (99.2% of released ^{39}Ar, MSWD = 44; Figure 7b). Again, two distinct parts can be distinguished in the spectrum. A low-temperature age of 11.05 ± 0.12 Ma is preserved in steps 2–5, while an age of 12.18 ± 0.15 Ma is shown by steps 6–9. The isochron age using 99.2% of released ^{39}Ar stands between these two ages (11.35 ± 0.37 Ma, MSWD = 2.2), which is consistent with the global plateau age.

The two sampled adularia crystals show a main crystallization stage at 11.4–11.5 Ma, with some older components in the two runs: older than 12 Ma and older than 14 Ma, respectively.

4.1.2. Sample MB03-70

Sample MB03-70_*grain 1* shows a plateau of 12.54 ± 0.34 Ma (MSWD = 11) integrating steps 2–10 (Figure 7c). The Ar spectrum shows a slight staircase shape for steps 2–3 (11.2–11.3 Ma) and steps 8–9 (14.6 Ma), followed by a slight descent on the last step (12.3 ± 0.5 Ma). The isochron plot yields an age of 11.3 ± 0.7 (MSWD = 2.74) in agreement with the lower temperature part of the $^{40}Ar/^{39}Ar$ plateau.

Sample MB03-70_*grain 2* shows a less well constrained plateau age of 13.07 ± 0.8 Ma, with an identical shape (Figure 7d). Steps 2–3 show a younger age of 11.6–12.4 Ma, and step 4 shows an age of 14.1 Ma, followed by a last step (step 7) at 12.8 ± 0.1 Ma. The isochron plot gives an age of 12.8 ± 0.8 Ma within error of the plateau age.

4.2. Aar Massif

4.2.1. Sample AA03-11

This sample provided a plateau age of 12.63 ± 1.55 Ma (MSWD = 5.88), but except for the last fusion step, it presents a spectrum with increasing ages toward higher-temperature steps (Figure 8a). At low temperature (steps 2–3), an age of 9–10 Ma is obtained, increasing toward ages of 14–16 Ma at high temperature (steps 8–10). The isochron age is in agreement with this upper age range (14.04 ± 1.18 Ma, MSWD = 0.81; Table 2).

Table 3. Isotope Compositions of Analyzed Minerals[a]

Samples	Calcite $\delta^{18}O$	Calcite $\delta^{13}C$	Quartz $\delta^{18}O$	Samples	Calcite $\delta^{18}O$	Calcite $\delta^{13}C$	Quartz $\delta^{18}O$	Samples	Calcite $\delta^{18}O$	Calcite $\delta^{13}C$	Quartz $\delta^{18}O$
Mont Blanc Crystalline Rocks				*Western Sediments*				*Aar Crystalline Rocks*			
S90 CC	18.50	−0.39	-	S70	20.74	−0.28	24.10	S11	-	-	10.32
PA 1	-	-	7.60	S73	17.28	−3.51	19.73	S 15	-	-	11.00
S80b	8.44	−6.72	11.34					S 28b	7.83	−7.69	9.93
MB 55	-	-	9.10					S29	-	-	10.42
MB 57	8.05	−10.02	9.76	*Eastern Sediments*				S35	-	-	10.42
C 31	8.81	−9.88	10.70	MB 153	8.80	−10.75	11.10	S 36	6.89	−9.02	9.76
S83	8.72	−6.47	11.75	MB 100	21.70	−0.89	21.94	S37	-	-	15.95
MB04 07	8.02	−4.09	10.50	MB 156	22.41	−1.78	23.03	S45	7.67	−8.28	10.62
MB04 08	8.70	−4.07	-	MB 105	21.77	3.90	21.82	S 46	7.98	−8.33	10.56
MB04 10	8.61	−4.11	10.80	MB 109	23.74	0.92	24.91	S48	-	-	10.32
MB 149	-	-	11.41	S95	17.85	−4.10	19.94	S48b	-	-	11.14
MB04 11	8.54	−3.81	10.70	S97c	18.63	−8.89	19.80	S50	-	-	10.01
S141 CC	23.86	−4.53	-	S 97	23.04	0.80	20.22	S 59	-	-	11.19
MB04 12	9.09	−4.17	11.50	S 99	23.97	1.58	27.21	S91 CC	10.70	−4.46	-
MB04 13	9.01	−3.59	-	S 102	21.54	−0.40	22.27	S 108	-	-	11.01
MB04 14	8.94	−2.77	-					S129	-	-	10.90
MB04 16	6.19	−5.35	8.50								
S140	10.61	−4.47	11.24								
MB04 22	6.07	−6.11	11.20								
MB04 24	7.89	−4.75	10.90								
SC 4	7.03	−4.45	11.31								
MB 99	9.85	−3.09	11.51								
MB 90	-	-	11.00								

[a] $\delta^{18}O$ in ‰ VSMOW; $\delta^{13}C$ in ‰ PDB.

4.2.2. Sample AA03-37

The laser $^{40}Ar/^{39}Ar$ experiment provided a flat spectrum featured by a plateau age of 11.51 ± 0.42 Ma (MSWD = 0.17, with 81.03% of degassed ^{39}Ar; Table 2). The isochron age is in agreement with the plateau age within the error margin (12.13 ± 0.39 Ma, MSWD = 0.99; Figure 8b). The inverse isochron (not shown) also provided meaningful results with an age of 11.00 ± 1.67 Ma (MSWD = 0.22). These ages show a good homogeneity of the sample apart from the first two steps, in which the age is younger (9–10 Ma).

5. Interpretation of Ar/Ar Dating of Vein Adularia

5.1. Mont Blanc Massif

Considering the Mont Blanc samples, $^{40}Ar/^{39}Ar$ spectra mostly show plateaus with quality criteria MSWD > 10 if plateau ages are computed with a majority of steps, which indicates that most steps in the $^{40}Ar/^{39}Ar$ spectra are not in agreement with a unique age. The whole data set agrees with an average crystallization age of 12.65 ± 1.48 Ma for a majority of signal (comprising 10 out of 34 steps) giving individual ages comprised between 11 and 12 Ma. Therefore, it seems that several ages have been preserved in the adularias, the principal crystallization stage being at 11–12 Ma. This is corroborated by the petrological features of adularias, which show a strong optical zoning in agreement with a multistage crystallization in the veins. Grains dated from the same veins have slightly different Ar/Ar ages, and distinct Ar isotopic ratios, in agreement with several stages of crystallization. Further, individual mineral Ar/Ar spectra yield complex shapes, which are not in agreement with a single stage of crystallization. If Ar/Ar spectra supposedly reflect contribution of the mineral rim at low temperature and increased contribution of the core at high temperature, the lower age steps reflect crystallization ages of 11–11.5 Ma, while core ages range from 12 to 16 Ma (i.e., steps 7–9 of sample MB08-22). As the dated phengites from neighboring shear zones, spatially associated with veins, gave $^{40}Ar/^{39}Ar$ ages of 15.8–16 ± 0.2 Ma [*Rolland et al.*, 2007, 2008], the most likely hypothesis to explain veins formation could be (1) veins opening as joints between shear zones and adularia crystallization onset starting at 16 Ma, followed by (2) acceleration of adularia growth at 12 Ma, and (3) end of adularia crystallization at 11 Ma. Subsequently, the veins would have remained opened to fluid flow for about 5 Ma.

Table 4. Isotope Compositions of Vein Chlorites

							δ^{18}O Equilibrium Fluid[c]		δD Equilibrium Fluid[b]	
	δ^{18}O	δD[a]		δD Chlorites	2σ		350°C	450°C	350°C	450°C
					Mont Blanc					
S80b	2.61	−56.6	−58.2	−55.0	-	2.3	3.29	4.32	−23.1	−25.5
MB 55	5.71	−67.2	−65.2	−69.1	-	2.7	6.39	7.43	−33.6	−36.1
MB 57	4.35	−68.3	−64.0	−71.0	−70.0	3.8	5.03	6.07	−34.8	−37.3
C 30	3.65	−65.1	−64.3	−66.0	-	1.2	4.33	5.37	−31.6	−34.1
C 31	2.75	−63.1	−65.2	−61.0	-	3.0	3.43	4.47	−29.6	−32.0
S83	3.65	−62.8	−64.5	−61.0	-	2.5	4.33	5.37	−29.2	−31.7
MB-04-07	4.50	−58.0	−58.0	-	-	-	5.18	6.22	−24.5	−26.9
MB-04-08	4.50	−57.0	−57.0	-	-	-	5.18	6.22	−23.5	−25.9
MB-04-10	4.30	−56.0	−56.0	-	-	-	4.98	6.02	−22.5	−24.9
MB 148	5.80	−62.5	−62.0	−63.0	-	0.7	6.48	7.52	−29.0	−31.4
MB 149	4.90	−74.4	−73.0	−75.9	-	2.0	5.58	6.61	−40.9	−43.3
MB-04-11	4.50	−61.0	−61.0	-	-	-	5.18	6.22	−27.5	−29.9
MB-04-12	5.20	−59.0	−59.0	-	-	-	5.88	6.92	−25.5	−27.9
MB-04-14	4.80	−63.0	−63.0	-	-	-	5.48	6.52	−29.5	−31.9
MB-04-22	4.90	−62.0	−62.0	-	-	-	5.58	6.62	−28.5	−30.9
MB-04-24	4.40	−60.0	−60.0	-	-	-	5.08	6.12	−26.5	−28.9
MB 94	4.59	−73.3	−73.0	−73.6	-	0.4	5.27	6.31	−39.7	−42.2
MB 96	0.60	−64.7	−60.0	−66.0	−68.0	4.2	1.28	2.32	−31.1	−33.6
MB 90	2.83	−70.1	−68.1	−72.0	-	2.7	3.51	4.54	−36.5	−39.0
					Aar					
S 15	3.33	−56.2	−56.5	−56.0	-	0.3	4.01	5.04	−22.7	−25.2
S 28b	2.51	−55.9	−53.7	−58.0	-	3.0	3.19	4.23	−22.3	−24.8
S29	2.61	−56.7	−56.5	−57.0	-	0.4	3.29	4.32	−23.2	−25.7
S35	2.30	−56.7	−55.5	−58.0	-	1.8	2.98	4.01	−23.2	−25.7
S 46	3.50	−60.1	−59.2	−61.0	-	1.3	4.18	5.22	−26.6	−29.0
S48	5.52	−63.0	−64.0	−62.0	-	1.4	6.20	7.23	−29.5	−31.9
S48b	3.19	−51.1	−52.1	−50.0	-	1.5	3.87	4.91	−17.5	−20.0
S50	3.64	−62.5	−62.9	−62.0	-	0.7	4.32	5.35	−28.9	−31.4
S 108	2.73	−51.4	−50.9	−52.0	-	0.8	3.41	4.44	−17.9	−20.4

[a]Average value of the different chlorites analyzed.
[b]Calculated using fractionation factors of *Graham et al.* [1984].
[c]Calculated using fractionation factors from *Wenner and Taylor* [1971].

5.2. Aar Massif

Despite the fact that both Aar adularia ^{40}Ar/^{39}Ar ages provide better constrained ages and MSWD values than the Mont Blanc samples, the results of sample AA03-11 are still not in agreement with a single age. The results are in agreement with crystallization of adularias between 14 and 11.5 Ma, with most single-step ages again ranging within 11–12 Ma. Given that the related shear zone phengites, spatially associated with these veins, have yielded ages of 12.2–13.8 ± 0.2 Ma [*Rolland et al.*, 2009], the age coincidence of vein adularia and shear zone phengite is clearly shown here. As for the MBM it is thus suggested that veins formed as joints to the main shear zones. Though, a tendency to have younger ages is shown in sample AA03-37, which suggests some delay between shear zone deformation and vein closure. Further, the staircase shape of sample AA03-11 could also indicate a progressive growth of this mineral between 14 and 9–10 Ma. This 9–10 Ma age is found in both samples for low-temperature steps and is interpreted as the last stage of mineral growth. In the Aar Massif, the data suggest fluid circulation in the opened veins for duration of about 4 to 5 Ma.

In both the Mont Blanc and the Aar Massifs, the main stage of fluid flow associated to vein formation is bracketed between 11 and 12 Ma. This time span is slightly younger than that estimated by *Mullis* [1996] from fluid inclusion in vein quartz (20–13 Ma) but is consistent with the formation of the youngest shear zones [*Challandes et al.*, 2008; *Rolland et al.*, 2009], thus dating the ductile-brittle transition.

6. Results of Stable Isotope Analysis

Stable isotope compositions of vein minerals are provided in Tables 3 and 4. Values of δ^{18}O and δ^{13}C of quartz, chlorite, and calcite are plotted in Figure 9 along a NW-SE transect through the MBM and its metasedimentary cover (Figure 2).

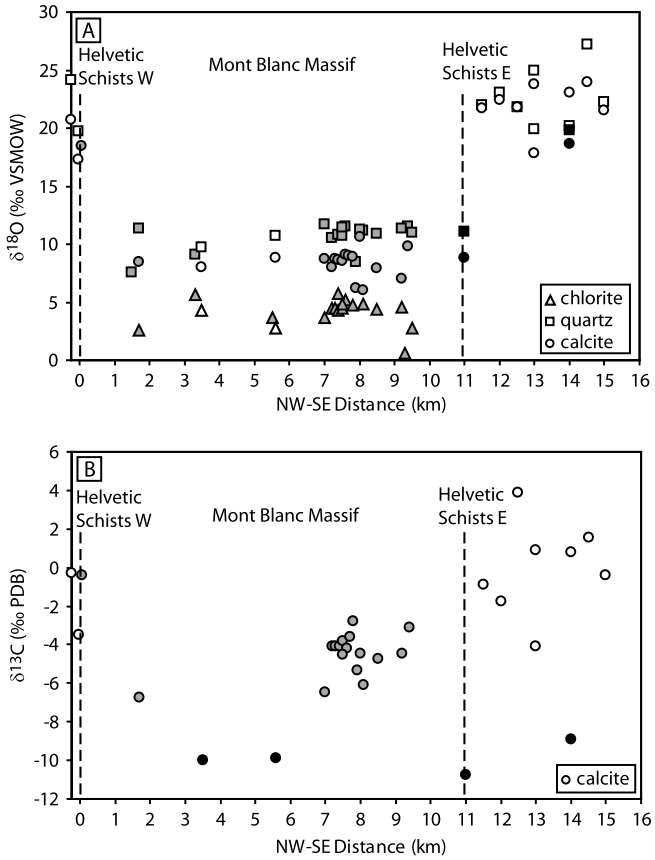

Figure 9. Stable isotope compositions of vein minerals reported along a NW-SE transect through the Mont Blanc Massif and its sedimentary cover. The horizontal axis represents the distance from the contact between the crystalline rocks and the sediments lying on the west side of the massif. (a) Values of $\delta^{18}O$ of quartz, chlorite, and calcite. (b) Values of $\delta^{13}C$ of calcite. Empty symbols represent A-type veins; grey symbols represent B-type veins; and black symbols represent C-type veins. The vein types are defined according to their $\delta^{13}C_{calcite}$ compositions (see text).

Based on oxygen isotope compositions, vein samples can be separated in two groups (Figures 9 and 10 and Tables 3 and 4): one group with high $\delta^{18}O$ values ($\delta^{18}O_{quartz}$ = +15.95 to +27.21‰, n = 12; $\delta^{18}O_{calcite}$ = +17.28 to +23.97‰, n = 13), and one group with much lower and homogeneous $\delta^{18}O$ values ($\delta^{18}O_{quartz}$ = +7.60 to +11.75‰, n = 33; $\delta^{18}O_{chlorite}$ = (+0.60) +2.61 to +5.80‰, n = 28 and $\delta^{18}O_{calcite}$ = +8.05 to +9.09‰, n = 23). With the exception of sample S90 CC hosted in basement rocks, and S141 CC, a vein calcite from the Mont Blanc granite, samples with high $\delta^{18}O$ values are hosted in the Helvetic metasediments (n = 12; Figure 9). With the exception of MB153, which is hosted in the sediments at the contact with the MBM, samples with low $\delta^{18}O$ values are all hosted in the Mont Blanc or the Aar crystalline rocks (n = 41; Figure 9).

Carbon isotope composition of vein calcite shows a large scatter, with values ranging from +3.90 down to −10.75‰ (Table 3 and Figure 9). With the exception of S97c ($\delta^{13}C$ = −8.89‰) and MB 153 ($\delta^{13}C$ = −10.75‰), all samples hosted in the Helvetic metasediments have carbon isotope compositions ranging between −4.10‰ and +3.90‰ (n = 11; Figure 9). In the Mont Blanc crystalline basement, most samples have $\delta^{13}C$ values ranging within −2.77‰ and −6.72‰ (n = 17), but two samples have very low $\delta^{13}C$ compositions: C31 ($\delta^{13}C$ = −9.88‰) and MB 57 ($\delta^{13}C$ = −10.02‰). Except sample S91 CC ($\delta^{13}C$ = −4.46‰), all calcite samples from the Aar Alpine veins have low $\delta^{13}C$ signature, ranging from −7.69‰ to −9.02‰. Low $\delta^{13}C$ compositions, which occur in the Mont Blanc and the Aar crystalline rocks and in the Helvetic metasediments as well, thus characterizes a third group of data.

In the MBM and in its metasedimentary cover, systematic variations in carbon and oxygen isotope compositions of vein calcite thus allow identification of three end-members (Figure 10): (1) A-type veins, with high $\delta^{18}O$ values ranging from +17.28 to +23.97‰ and $-4.10‰ \le \delta^{13}C \le +3.90‰$, (Helvetic and Valaisan metasediments, $n = 9 + 1$); (2) B-type veins, with low $\delta^{18}O$ ranging from +6.07 to +10.61‰ values and intermediate composition between A and C types: $-6.72 \le \delta^{13}C \le -2.77‰$ (Mont Blanc crystalline rocks; n = 17); and (3) C-type veins, with $\delta^{18}O$ values similar to those of calcite occurring in the same host rocks and $-8.89 \le \delta^{13}C \le -10.75‰$ (n = 4). These veins occur in association with deep-seated features: (i) the Mg-rich metasomatic zone from the central part of the MBM (C31), (ii) the Mg-rich metasomatic zone located along the Penninic Front (S97 CC), (iii) at the contact between the granite and the metasediments (MB153), and (iv) along a major shear zone in the gneissic basement (MB57).

Even though a few exceptions exist (e.g., sample S141 CC), there is an almost continuous distribution in the carbon isotope compositions of vein minerals between these three end-members (Figure 9). In the Aar

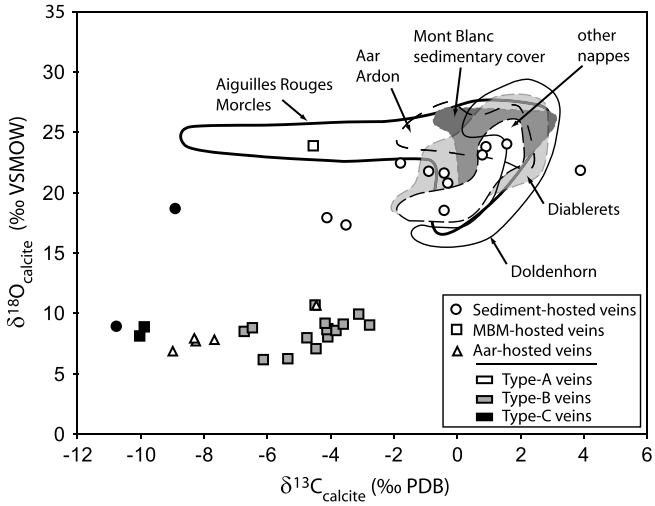

Figure 10. Plot of the $\delta^{13}C$ versus $\delta^{18}O$ values of vein calcite. Circles represent samples from the Mont Blanc sedimentary cover; squares represent samples from the Mont Blanc granite; and triangles represent samples from the Aar granodiorite. Empty symbols represent A-type veins; grey symbols represent B-type veins; and black symbols represent C-type veins. Stable isotope data from the Helvetic nappes and the Mont Blanc sedimentary cover reported from *Dietrich et al.* [1983], *Crespo-Blanc et al.* [1995], and *Kirschner et al.* [1999] are shown as fields.

Massif, vein calcites range between the MBM B-type and C-type veins, thus filling gap between these two end-members (Figure 10).

Hydrogen stable isotope of chlorite was analyzed in veins hosted in crystalline rocks. The average hydrogen isotope composition of the Aar chlorites (−51.1‰ to −63.0‰) is slightly higher than that of the Mont Blanc chlorites (−56.0‰ to −75.6‰, Table 4). In both massifs, the hydrogen isotope composition of chlorites is not linearly correlated to the oxygen isotope composition (+0.6‰ and +5.8‰ respectively, Figure 11a).

7. Interpretation of Stable Isotope Data

Reactive fluid was responsible for precipitation of minerals in veins and alteration of the surrounding wall rocks to create alteration haloes [*Rossi et al.*, 2005]. Comparison of the stable isotope values measured with those of potential fluid sources might allow determination of the origin of the reactive fluid for the different identified vein types.

7.1. Comparison With Data From the Helvetic Alps

In veins hosted in the Helvetic metasediments (A-type veins), the oxygen isotope composition of quartz is similar to that measured by *Crespo-Blanc et al.* [1995] on the eastern side of the MBM. With the exception of a few samples, most oxygen isotope compositions of calcite plot in the field defined by the Helvetic nappes ($\delta^{18}O_{calcite}$ = +16‰ to +28‰, Figure 10) [*Dietrich et al.*, 1983; *Crespo-Blanc et al.*, 1995; *Kirschner et al.*, 1999]. However, $\delta^{13}C$ values of A-type calcite follow a trend from the average isotopic composition of the Helvetic nappes toward lower carbon isotope compositions of C-type end-member (Figure 10). This trend is rather well correlated with the field defined in the Diablerets nappe in the vicinity of its basal thrust [*Crespo-Blanc et al.*, 1995]. Possible explanations for this trend are discussed in section 8.2.

In veins hosted in crystalline rocks, quartz, chlorite, and calcite have rather homogeneous $\delta^{18}O$ compositions. Except for PA1 ($\delta^{18}O_{quartz}$ = +7.6‰) and MB04-16 ($\delta^{18}O_{quartz}$ = +8.5‰), the oxygen isotope composition of vein quartz (from +9.1‰ to +11.7‰) is consistent with values of vein quartz hosted in the Mont Blanc basement and in other external crystalline massifs of the Alps ($\delta^{18}O_{quartz}$ = +9.0‰ to +15.3‰) [*Hoernes and Friedrichsen*, 1980; *Fourcade et al.*, 1989; *Marshall et al.*, 1997, 1998]. These values are also similar to those of crystalline quartz from the Aiguilles Rouges gneisses ($\delta^{18}O_{quartz}$ = +10.9‰ to +12.4‰) [*Marquer et al.*, 1994] and of magmatic quartz in plutonic granites and granodiorites ($\delta^{18}O_{quartz}$ = +9.0‰ to +12.5‰) [*Taylor*, 1968]. The $\delta^{18}O$ values of chlorite are close to those measured in other external crystalline massifs [*Hoernes and Friedrichsen*, 1980]. Finally, oxygen isotope compositions of vein calcite are close to those measured within the metamorphic basement and related tectonic veins: $\delta^{18}O_{calcite}$ = +8.70‰ to +9.20‰ in the basement marbles, while $\delta^{18}O_{calcite}$ = +7.97‰ to +8.20‰ within associated veins [*Marshall et al.*, 1997, 1998].

Hydrogen isotope compositions of vein chlorites range between the field defined by the compositions of micas from the Helvetic schists and the meteoric water line (Figure 11b). In the Aar Massif, δD values of vein chlorites are similar to those of granitic biotites [*Hoernes and Friedrichsen*, 1980] suggesting that hydrogen is being buffered by the host rock. The H_2O-rich fluid could thus either derive from biotite dissolution in the vein's alteration halo or derive from devolatilization of the Helvetic schists. In this later case, the fluid/rock ratio must be

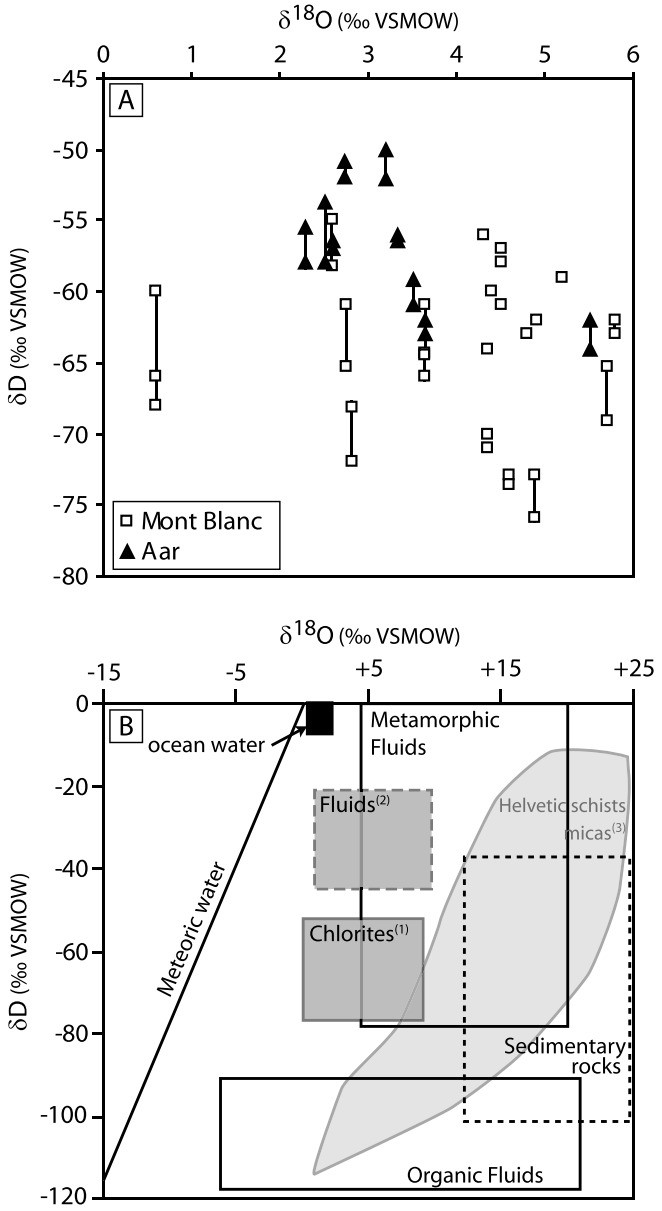

Figure 11. (a) Hydrogen versus oxygen isotopic compositions of vein chlorites (B-type veins) from the Mont Blanc (squares) and the Aar (triangles) crystalline rocks. Different chlorite analyses from the same samples are connected by a vertical bar to show the spread of the δD compositions in the samples. Standard deviations (2σ) are 2‰ for δD values and 0.2‰ for δ^{18}O values. (b) Comparison of data from this study (field 1) with the fields of ocean water, meteoric water, metamorphic fluids, organic fluids, and sedimentary rocks [after *Sheppard*, 1986]. Field 2 represents the range of δD and δ^{18}O values of the fluid in equilibrium with chlorites at 350–450°C (fractionation curves of *Graham et al.* [1984] and *Zheng* [1999]) and field 3 the range of δD and δ^{18}O values of micas from the Helvetic schists [*Hunziker et al.*, 1986; *Burkhard et al.*, 1992; *Crespo-Blanc et al.*, 1995].

low so that hydrogen became buffered by the veins' host rocks. As the fluid in equilibrium with the Alpine chlorites plots between the fields defined by metamorphic waters and the meteoric water line, it is likely that vein chlorites precipitated from a metamorphic locally derived fluid, involving some mixing with or late circulation of a meteoric fluid. In the Mont Blanc Massif, *Rossi et al.* [2005] identified two sets of vein chlorites (green vermicular chlorites and oxidized chlorites), thus confirming that late alteration from meteoric waters occurred.

C-type veins have low δ^{13}C values, which have not been reported in vein calcite hosted in the Helvetic schists so far. The origin of the fluid responsible for such low δ^{13}C values is discussed in section 8.3.

7.2. Isotopic Equilibrium Versus Disequilibrium Among Vein Minerals

Minerals in isotopic equilibrium may either have crystallized from a single fluid or have crystallized from different fluids and later been equilibrated. In such a case, the use of isotopic geothermometers should provide realistic fluid temperatures. On the other hand, minerals in isotopic disequilibrium may either have crystallized initially from different fluids or have precipitated originally from the same fluid with the different minerals having reequilibrated at various postcrystallization temperatures. It is also possible that some of the minerals exchanged with a later fluid, resulting in nonequilibrium isotopic compositions. In such cases, the use of isotopic geothermometers should provide unrealistic or meaningless fluid temperatures.

In veins hosted in the Mont Blanc and the Aar crystalline rocks, the quartz-calcite geothermometer of *Zheng* [1999] gives fluid temperature estimates lower than 200°C (Figure 12b). Such very low fluid temperatures are clearly underestimated as temperatures calculated from fluid inclusions trapped in vein quartz range from 350°C to 420°C [*Poty*, 1969; *Poty et al.*, 1974; *Fabre et al.*, 2002]. Vein quartz and vein calcite are thus not in isotopic equilibrium, which is consistent with field observations.

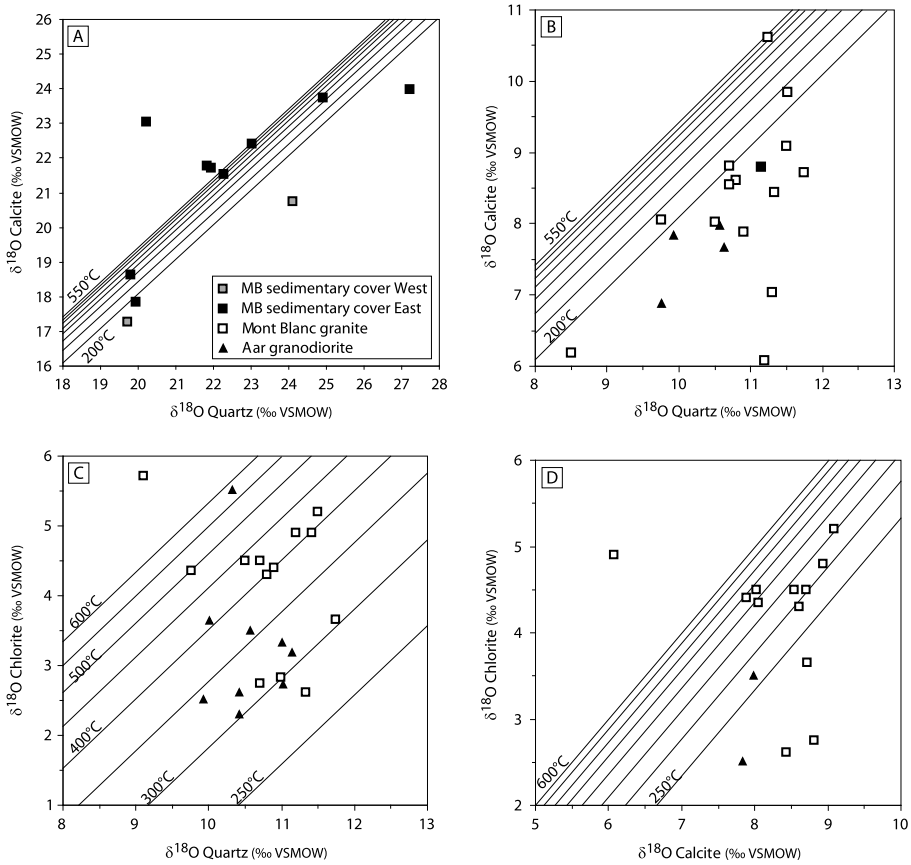

Figure 12. (a) Plot of $\delta^{18}O_{quartz}$ versus $\delta^{18}O_{calcite}$ for veins hosted in the Mont Blanc sedimentary cover. Isotherms were calculated using the geothermometer of *Zheng* [1999]. (b) Plot of $\delta^{18}O_{quartz}$ versus $\delta^{18}O_{calcite}$ of veins hosted in the Mont Blanc and the Aar crystalline rocks. Note that sample MB 153, which was sampled within the sedimentary cover close to the contact with the granite, shows isotopic compositions similar to those of veins hosted in the Mont Blanc granite. (c) Plot of $\delta^{18}O_{quartz}$ versus $\delta^{18}O_{chlorite}$ of samples hosted in the Mont Blanc and the Aar crystalline rocks. Isotherms were calculated using the geothermometer of *Wenner and Taylor* [1971]. (d) Plot of $\delta^{18}O_{calcite}$ versus $\delta^{18}O_{chlorite}$ of samples hosted in the Mont Blanc and the Aar crystalline rocks. Isotherms were calculated by coupling the geothermometers of *Wenner and Taylor* [1971] and of *Zheng* [1999].

With the exception of a few samples, most fluid's temperatures estimated in veins hosted in the Mont Blanc sedimentary cover using the quartz-calcite geothermometer of *Zheng* [1999] are either overestimated or underestimated, yielding temperatures with no geological meaning (Figure 12a). As for veins hosted in the crystalline rocks, quartz, and calcite thus appear not to be in isotopic disequilibrium.

In most veins hosted in the Mont Blanc and the Aar crystalline rocks, fluid temperatures estimated using the quartz-chlorite geothermometer of *Wenner and Taylor* [1971] range between 280°C and 440°C. However, in the MBM, two distinct crystallization stages may be distinguished (Figure 12c). The first crystallization stage occurred at temperatures ranging between 400 and 440°C, which are consistent with temperatures estimated during peak metamorphism in the shear zones [*Rolland et al*., 2003; *Rossi et al*., 2005; *Challandes et al*., 2008] and with temperatures calculated in Alpine veins from fluid inclusion studies [*Poty*, 1969; *Poty et al*., 1974]. The second crystallization stage occurred at temperatures of 280–350°C, which is also consistent with temperatures calculated in Alpine veins from fluid inclusion studies or using the thermodynamic properties of vein minerals [*Fabre et al*., 2002; *Rossi et al*., 2005]. Vein quartz and vein chlorite may thus have reached isotopic equilibrium; their relationships in veins suggesting contemporaneous crystallization (Figure 5). These isotopic data confirm the multistage filling of the Alpine veins, as already suggested by *Rossi et al*. [2005] using the chlorite solid-solution model and thermodynamic data from *Vidal et al*. [2001] as well as the thermometers of *Cathelineau and Nieva* [1985] and *Hillier and Velde* [1992]. Unlike the MBM, in the Aar Massif, the continuous trend in Figure 12c suggests

Table 5. Calculated Isotope Composition of H_2O and CO_2 in Equilibrium With Vein Quartz and Vein Calcite

	$\delta^{13}C_{CO2}$ (‰ PDB)	$\wedge\delta^{18}O^{CO2}$ (‰ VSMOW)	$\delta^{18}O_{H2O}$(‰ VSMOW)				
	(Calcite)	(Calcite)	(Calcite)	(Quartz)			
	Chacko et al. [1991]	*Chacko et al.* [1991]	*Zheng* [1999]	*Zheng* [1993]			
	300°C	300°C	300°C	300°C	350°C	400°C	450°C
			Mont Blanc Massif				
			Type A Veins				
S70	2.62	29.30	14.95	17.07	18.50	19.59	20.42
S73	−0.61	25.84	11.49	12.70	14.14	15.22	16.05
MB 100	2.01	30.26	15.91	14.91	16.35	17.43	18.26
MB 156	1.12	30.97	16.62	16.00	17.43	18.51	19.34
MB 105	6.80	30.33	15.97	14.79	16.22	17.31	18.14
MB 109	3.82	32.30	17.95	17.88	19.32	20.40	21.23
S95	−1.20	26.41	12.06	12.91	14.34	15.43	16.26
S 97	3.70	31.60	17.24	13.19	14.62	15.71	16.54
S 99	4.48	32.53	18.18	20.18	21.61	22.70	23.53
S 102	2.50	30.10	15.75	15.24	16.68	17.76	18.59
			Type B Veins				
S90 CC	2.51	27.06	12.71	-	-	-	-
PA 1	-	-	-	0.57	2.00	3.08	3.91
S80b	−3.82	17.00	2.64	4.31	5.74	6.83	7.66
MB 55	-	-	-	2.07	3.51	4.59	5.42
S83	−3.57	17.28	2.92	4.72	6.15	7.24	8.07
MB-04-07	−1.19	16.58	2.23	3.47	4.90	5.99	6.82
MB-04-08	−1.17	17.26	2.91	-	-	-	-
MB-04-10	−1.21	17.17	2.82	3.77	5.20	6.29	7.12
MB 149	-	-	-	4.38	5.81	6.90	7.73
S141 CC	−1.63	32.42	18.06	-	-	-	-
MB-04-11	−0.91	17.10	2.75	3.67	5.10	6.19	7.02
MB-04-12	−1.27	17.65	3.30	4.47	5.90	6.99	7.82
MB-04-13	−0.69	17.57	3.22	-	-	-	-
MB-04-14	0.13	17.50	3.15	-	-	-	-
MB-04-16	−2.45	14.75	0.40	1.47	2.90	3.99	4.82
S140	−1.57	19.17	4.82	4.21	5.64	6.72	7.55
MB-04-22	−3.21	14.63	0.28	4.17	5.60	6.69	7.52
MB-04-24	−1.85	16.45	2.10	3.87	5.30	6.39	7.22
SC 4	−1.55	15.59	1.24	4.28	5.71	6.79	7.62
MB 99	−0.19	18.41	4.06	4.48	5.92	7.00	7.83
MB 90	-		-	3.97	5.40	6.48	7.31
			Type C Veins				
MB 57	−7.12	16.61	2.26	2.73	4.16	5.25	6.08
C 31	−6.98	17.37	3.02	3.67	5.10	6.19	7.02
MB 153	−7.85	17.36	3.01	4.07	5.50	6.59	7.42
S97c	−5.99	27.19	12.84	12.77	14.20	15.29	16.12
			Aar Massif				
S11	-	-	-	3.29	4.72	5.80	6.63
S 15	-	-	-	3.97	5.41	6.49	7.32
S 28b	−4.79	16.39	2.04	2.90	4.33	5.41	6.24
S29	-	-	-	3.39	4.82	5.91	6.74
S35	-	-	-	3.39	4.82	5.91	6.74
S 36	−6.12	15.45	1.10	2.73	4.16	5.25	6.08
S37	-	-	-	8.92	10.35	11.43	12.26
S45	−5.38	16.23	1.88	3.59	5.03	6.11	6.94
S 46	−5.43	16.54	2.19	3.53	4.97	6.05	6.88
S48	-	-	-	3.29	4.72	5.80	6.63
S48b	-	-	-	4.11	5.54	6.62	7.45
S50	-	-	-	2.98	4.41	5.50	6.33
S 59	-	-	-	4.16	5.59	6.68	7.51
S91 CC	−1.56	19.26	4.91	-	-	-	-
S 108	-	-	-	3.98	5.42	6.50	7.33
S129	-	-	-	3.87	5.30	6.39	7.22

a more continuous crystallization of vein minerals (quartz and chlorite) under decreasing temperatures from 400°C to 300°C.

7.3. Calculated Fluid's Isotopic Composition

The oxygen isotope composition of H_2O in equilibrium with vein quartz was calculated using the temperature-dependent quartz-H_2O fractionations of *Zheng* [1993] for the temperature range 300-450°C. As calcite crystallizes in a later stage, after the two stages of quartz and chlorite filling, we can assume that calcite crystallizes at a temperature lower than 300°C. Therefore, the isotopic composition of the fluid in equilibrium with vein calcite was calculated at a temperature of 300°C, in order to give insights of its maximum values. The oxygen isotope composition of the H_2O-rich fluid in equilibrium with vein calcite was calculated using the temperature-dependent calcite-H_2O fractionations of *Zheng* [1999], and the carbon isotope composition of CO_2 was calculated using the temperature-dependant calcite-CO_2 fractionations of *Chacko et al*. [1991]. All data are presented in Table 5.

With the exception of sample MB153, all vein quartz hosted in the Mont Blanc metasedimentary cover have high $\delta^{18}O$ values. These quartz crystals crystallized from a H_2O-rich fluid with $\delta^{18}O_{H2O}$ values ranging from +12.70‰ to +17.88‰ at 300°C to +16.05‰ to +21.23‰ at 450°C (sample S99 crystallized from a fluid with slightly higher $\delta^{18}O_{H2O}$ values). Such high values suggest infiltration of H_2O-rich fluid in equilibrium with sedimentary rocks. With the exception of sample S37 (Aar Massif), all vein quartz hosted in the Mont Blanc and the Aar crystalline rocks have low $\delta^{18}O$ values. The $\delta^{18}O$ values of the H_2O-rich fluid in equilibrium with these vein quartz range between +0.57‰ to +4.72‰ at 300°C and +3.91‰ to +8.07‰ at 450°C. Such isotopic compositions are consistent with those of H_2O-rich fluid in equilibrium with crystalline rocks. The oxygen isotope composition of the fluid from which vein quartz crystallized is thus apparently buffered by the vein's host rock (see section 8.1 for discussion). Assuming calcite precipitated at a maximum temperature of 300°C, the calculation of the fluid $\delta^{18}O_{H2O}$ values range between +11.49‰ and +18.18‰ for veins hosted in the Mont Blanc metasedimentary cover, and between +0.28‰ and +4.91‰ for veins hosted in the Mont Blanc and the Aar crystalline rocks. As for vein quartz, the oxygen isotope composition of the H_2O-rich fluid from which calcite crystallized seems to be buffered by the vein's host rock.

As the crystalline rocks do not contain any significant carbon, calcite occurrence in veins hosted in crystalline rocks necessarily involves infiltration of an external H_2O-CO_2-rich fluid. In the Mont Blanc metasedimentary cover, vein calcite (A-type) equilibrated at 300°C with a fluid which $\delta^{13}C_{CO2}$ values range between −1.20‰ and +6.80‰, and $\delta^{18}O_{CO2}$ values range between +25.84‰ and +32.53‰. Such high carbon isotope signatures are consistent with a H_2O-CO_2-rich fluid derived from sedimentary rocks. In B-type veins hosted in the Mont Blanc Massif, the $\delta^{13}C_{CO2}$ and $\delta^{18}O_{CO2}$ values of the H_2O-CO_2-rich fluid in equilibrium with vein calcite at 300°C range respectively between −3.82‰ and +0.13‰ and between +14.63‰ and +19.17‰. Calcites from C-type veins have the lowest carbon isotope composition. They equilibrated at 300°C with a H_2O-CO_2-rich fluid, which $\delta^{13}C_{CO2}$ values range between −7.85‰ and −5.99‰. As for $\delta^{18}O_{H2O}$, the $\delta^{18}O_{CO2}$ values of C-type veins were buffered by the vein's host rock. Vein calcites from the Aar Massif show intermediate values (between B-type and C-type veins). They crystallized in equilibrium at 300°C with a H_2O-CO_2-rich fluid which $\delta^{13}C_{CO2}$ values range between −5.84‰ and −1.28‰, and the $\delta^{18}O_{CO2}$ values range between +15.45‰ and +19.26‰. Vein calcites hosted in the Mont Blanc and the Aar crystalline rocks therefore suggest infiltration of a H_2O-CO_2-rich fluid with a more or less ^{13}C-depleted signature.

8. Discussion

Stable isotopes were analyzed in Alpine vein minerals associated with shear zones and faults in the Mont Blanc and Aar Massifs and in their sedimentary cover in order (1) to examine the structural controls on fluid redistribution between fluid reservoirs during the Alpine deformation, (2) to place constraints on the composition and distribution of the fluid reservoirs, and (3) to determine the scales of fluid redistribution that drove fluid-rock interactions and mass transfer within the continental crust during Alpine deformation.

8.1. Fluid Reservoirs: Fluid-Buffered Versus Host Rock-Buffered Fluid

In order to identify the possible fluid reservoirs and the scale of fluid flow during the development of Alpine shear zones and associated veins, isotopic, chemical, and geological data are used to discuss the roles of local

host rock buffering versus external fluid sourcing in vein formation in the ECM and in their metasedimentary cover. Two fluid sources may explain that vein minerals precipitated from a fluid with $\delta^{18}O$ values in equilibrium with the vein's host rock: (i) a locally derived fluid or (ii) an external fluid with low fluid/rock ratio, so that the fluid's oxygen isotope composition was buffered by the vein's host rock during fluid flow.

8.1.1. Helvetic Schists Veins

In the Helvetic schists, the oxygen and carbon isotope compositions of vein calcite and vein quartz evolve from typical Helvetic carbonates values toward lower values (Figure 10). As A-type vein minerals crystallized from a H_2O-CO_2-rich fluid in isotopic equilibrium with sedimentary rock, this trend suggests that calcite crystallized from a locally derived fluid for which carbon and oxygen isotope compositions were slightly depleted. The Helvetic metasediments (Jurassic shales, marls, and limestones) of the Mont Blanc sedimentary cover and the Morcles nappe thus constitute a possible reservoir for this H_2O-CO_2-rich fluid.

8.1.2. Mont Blanc Veins

In the MBM, vein quartz and vein chlorite crystallized from a H_2O-rich fluid in isotopic equilibrium with crystalline rocks. This mineralizing fluid is either locally derived (i.e., derived from the vein's host rock) or represents an external H_2O-rich fluid with a low fluid-rock ratio that underwent later oxygen isotope exchange and reequilibration with the crystalline host rock. Evidences of vein formation involving a locally derived H_2O-rich metamorphic fluid in a relatively closed system are provided (1) by the composition of fluid inclusions trapped in vein quartz, which are H_2O-rich with generally less than 2% CO_2 [e.g., *Poty*, 1969; *Poty et al*., 1974; *Fabre et al*., 2002], and (2) by mass balance calculation, which indicates that the amount of quartz and chlorite that precipitate in Alpine veins is balanced by the amount of quartz and biotite that was dissolved in the alteration haloes around the veins [*Rossi*, 2005]. The crystallization of vein minerals in a nearly closed system has already been invoked by several authors in the crystalline and sedimentary rocks of the Western Alps [*Fourcade et al*., 1989; *Marquer and Burkhard*, 1992; *Henry et al*., 1996].

As calcite is the last mineral to crystallize in the MBM veins and as it appears not to be in isotopic equilibrium with the other vein minerals (Figure 12), filling of alpine veins with a quartz + chlorite ± calcite assemblage thus implies at least two episodes of fluid-rock interactions: (1) precipitation of quartz + chlorite ± adularia from a H_2O-rich fluid and (2) a later infiltration of a H_2O-CO_2-rich fluid that crystallizes calcite. Since the granite is carbon free, the presence of calcite in some veins implies infiltration of an external H_2O-CO_2-rich fluid, in which oxygen isotope composition is buffered by the granite and carbon isotope composition is buffered by the fluid. Therefore, the $\delta^{13}C$ values of calcite in B- and C-type veins give insights on this external H_2O-CO_2-rich fluid's composition, which origin will be discussed in section 8.3.

8.1.3. Aar Veins

Alpine veins from the Aar Massif have oxygen isotope compositions buffered by crystalline host rock and carbon isotope compositions ranging between those of the Mont Blanc B-type and C-type veins, suggesting the infiltration of a ^{13}C-depleted CO_2-rich fluid ($\delta^{13}C_{CO2}$ from −5.84‰ to −1.28‰). Two fluid-rock interaction episodes may be invoked for the veins formation, like for the MBM B-type and C-type veins.

8.2. Origin of the C-O Decrease in Veins Hosted in the Helvetic Metasediments

Three mechanisms may explain the trend observed in A-type veins ranging from high $\delta^{13}C$-$\delta^{18}O$ values typical of the Helvetic nappes toward lower $\delta^{13}C$-$\delta^{18}O$ values measured in calcite from the metasomatic zone observed in the Helvetic schists (C-type calcite): (1) calcite decarbonation and devolatilization [e.g., *McCrea*, 1950; *Nabelek et al*., 1984], (2) variable degrees of rock buffering and fluid-rock interaction [e.g., *Taylor*, 1977; *Nabelek*, 1987; *Dipple and Ferry*, 1992], and (3) mixing of two different fluids: a fluid with high-$\delta^{13}C$-$\delta^{18}O$ compositions released during compaction of the sedimentary sequence and an externally derived fluid with low $\delta^{13}C$ values.

Decarbonation reactions occurred during metamorphism of the Helvetic schists (see *Livi et al*. [2000] for a review of the metamorphic reactions in the Liassic black shales and marls) producing ^{13}C-rich CO_2 relative to the remaining carbonate, thus leading to a significant lowering of the $\delta^{13}C$ values of calcite [*Lattanzi et al*., 1980; *Valley*, 1986; *Nabelek et al*., 1984; *de Oliveira and Santos*, 2003]. Assuming vein calcite is at equilibrium with the Helvetic schists [*Dietrich et al*., 1983], decarbonation reactions could explain part of the variability of the carbon isotope composition observed in the A-type veins. However, it fails to explain the low $\delta^{13}C$ values observed in some B-type veins (MB 156, S95) and in the C-type vein (S97c). Calcite decarbonation alone thus fails to explain the shift and the variability observed in the C-O isotope compositions of A-type veins.

Similar decrease of $\delta^{13}C$ values is documented by *Crespo-Blanc et al.* [1995] and *Burkhard et al.* [1992] from the foreland toward the hinterland part of the Helvetic nappes in both Diablerets and Glarus thrusts. This lowering has been interpreted as a progressive alteration effect of the locally derived fluid isotopic composition by interaction with carbonates along the fluid's pathway or as the effect of dispersion of a ^{13}C-depleted fluid from the main thrust contact [*Baumgartner and Rumble*, 1988; *Crespo-Blanc et al.*, 1995]. Similarly, we propose that the decreasing trend of C-O isotope compositions evidenced in A-type veins (Figure 10) indicates variable degrees of fluid-rock interactions and mixing between a locally derived fluid and an externally derived fluid, which has a low-$\delta^{13}C$ composition and must be related to C-type veins. The apparent scatter observed in $\delta^{13}C$ and $\delta^{18}O$ values in Figures 9 and 10 thus probably reflects various degrees of buffering by both A-type and C-type end-members.

8.3. Fluid Mixing and the Origin of Carbon in the Mont Blanc and the Aar Massifs

In the MBM, $\delta^{13}C$ values of B-type veins range from the high $\delta^{13}C_{A\text{-type}}$ values found in the Helvetic schists to the low $\delta^{13}C_{C\text{-type}}$ values found in the center of the MBM (Figures 9b and 10), thus defining a continuous trend of lowering $\delta^{13}C$ values from the Helvetic schists to the center of the MBM. From discussion in section 8.2, it appears very unlikely that calcite from the external crystalline massif precipitated from a H_2O-CO_2-rich fluid derived from the sedimentary cover only. One possibility would imply low-temperature ($<$185°C) fractional precipitation of calcite from the ECM contact, which would drive the fluid's composition to a lower value of $\delta^{13}C$. Even though Figure 9 could illustrate such a process, it is most likely not a dominant process. Vein quartz and vein chlorite precipitate at temperatures of 300°C to 450°C (Figure 12). If calcite formed closely after the other vein minerals, it would precipitate at a rather high temperature (200–300°C), and carbon fractionation factor $1000\ \ln\alpha_{cc\text{-}CO2}$ would be negative [*Chacko et al.*, 1991]. In such a case, the $\delta^{13}C$ signature of calcite hosted in crystalline rocks should increase from the contact, which is not consistent with the data. For calcite to precipitate at temperatures below 185°C, the veins must thus be closed for some time and reopen in a later stage. However, the location of C-type veins requires another explanation as (i) these veins occur in the central part of the massif as well as at the contact with the Helvetic cover and (ii) they are closely related to deep-seated geological structures:

1. S97c vein was sampled along the Mg-rich metasomatic zone that underlines the Penninic Front putting into contact the (high pressure metamorphic) Valais zone with the slightly metamorphosed Mont Blanc metasedimentary cover.
2. MB153 vein was sampled along the Mont Blanc back thrust (at the contact between the Mont Blanc granite and its sedimentary cover).
3. MB57 vein was sampled in the vicinity of a main thrust within the Mont Blanc metamorphic basement, and C31 was sampled in a vein associated with the Mg-rich metasomatic high-strain zone identified by *Rossi et al.* [2005] in the center of the Mont Blanc granite.

A more likely explanation of $\delta^{13}C_{B\text{-type}}$ values implies variable rock buffering and mixing of a high- $\delta^{13}C$ fluid buffered by the Helvetic schists (A-type veins), with a low-$\delta^{13}C$ external fluid (C-type veins). Such mixing suggests fluid infiltration from the sedimentary cover to the MBM, as well as fluid flow at a larger scale as evidenced by the infiltration of an externally buffered fluid. Two explanations have been proposed to explain the very low $\delta^{13}C$ compositions in C-type carbonates (i.e., ^{13}C-depleted fluid): (1) interaction with a CH_4-rich fluid derived from organic-rich carboniferous sediments ($\delta^{13}C_{CO2} < -25‰$, for example) [*Hoefs*, 1987; *Rollinson*, 1993; *Kotarba and Clayton*, 2003] and (2) interaction with a deep-seated CO_2-rich fluid derived from or modified by interaction with upper mantle or lower crust rocks ($\delta^{13}C_{CO2} = -5$ to $-8‰$) [*Javoy et al.*, 1986; *Kyser*, 1986; *Cartigny et al.*, 2001].

1. In the Helvetic metasedimentary cover, organic carbon is documented in fluid inclusions [*Frey et al.*, 1980; *Mullis et al.*, 1994] and in organic matter [*Kirschner et al.*, 1999]. In the Mont Blanc area, organic carbon is only documented in two samples from the Helvetic cover of the MBM ($\delta^{13}C_{organic} = -14.7‰$ and $-15.9‰$) [*Kirschner et al.*, 1999]. According to fractionation factors of *Horita* [2001], at 350–450°C, the fluid in isotopic equilibrium with this organic carbon would have $+0.02‰ < \delta^{13}C_{CO2} < +5.54‰$. In the Mont Blanc crystalline rocks, no hydrocarbons were described in the fluid inclusions trapped in Alpine veins [*Poty*, 1969; *Poty et al.*, 1974; *Fabre et al.*, 2002]. However, *Marshall et al.* [1997] described graphite in marble lenses hosted in the Variscan gneissic basement of the northern Mont Blanc Massif ($\delta^{13}C_{graphite} = -10.77$ to $-7.33‰$). Using the fractionation factors of *Chacko et al.* [1991] at 350°C and 450°C, the fluid in

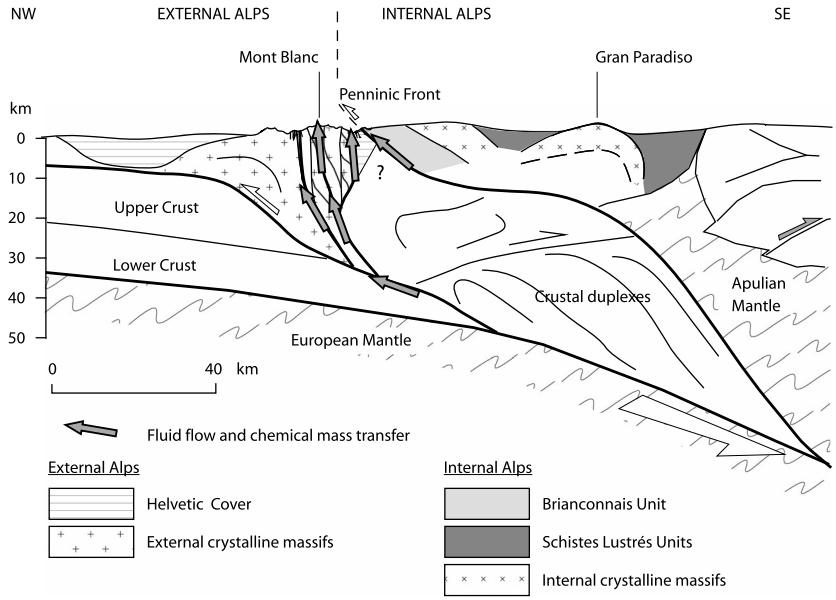

Figure 13. Interpreted crustal-scale fluid pathways (grey arrows) in the crystalline basement of NW Alps (from the example of the Mont Blanc) at about 14–11 Ma. The fluid pathways and associated chemical mass transfer are deduced from the stable isotope studies of vein minerals. Geological cross section from ECORS-CROP seismic data, modified after *Roure et al.* [1996].

equilibrium with this graphite composition would have $+2.43‰ < \delta^{13}C_{CO2} < +8.99‰$ at 350–450°C. Such values of $\delta^{13}C_{CO2}$ are much higher than the composition of the fluid in equilibrium with C-type veins ($\delta^{13}C_{CO2}$ from $-7.85‰$ to $-5.99‰$) but are similar to the composition of the fluid in equilibrium with A-type veins (Table 5). Furthermore, if the ^{13}C-depleted fluid which formed the C-type veins derived from interaction with organic matter hosted in the Helvetic sediments, one would expect to find widespread C-type veins within the metasediments, and not only along deep-seated geological structures. It is thus very unlikely that C-type veins result from the infiltration of a ^{13}C-depleted fluid that interacted with graphite or organic matter hosted in the Helvetic sediments.

2. Deep-seated CO_2 has rather homogeneous $\delta^{13}C$ compositions ranging mainly from $-5‰$ to $-8‰$ in carbonatites, diamonds, MORB, deep crust, and subduction zones [*Javoy et al.*, 1986; *Kyser*, 1986; *Cartigny et al.*, 2001; *Deines*, 2002]. Such values are very similar to those estimated for the fluid in isotopic equilibrium with C-type calcite at 300°C ($-7.85‰ < \delta^{13}C_{CO2} < -5.99‰$) [*Chacko et al.*, 1991]. Furthermore, the crustal scale Alpine structure is favorable to the channelization of such a deep-seated fluid flowing upward along deep-seated structures such as the Penninic Front or the Mont Blanc back thrust, where C-type veins were sampled (Figure 13). Composition of C-type veins thus likely results from the infiltration of a deep-seated ^{13}C-depleted fluid. Moreover, two C-type samples (C31 and S97c) were associated with Mg metasomatism, which is consistent with the hypothesis of a deeply seated fluid buffered by mantle-derived rocks [*Ferrando*, 2012, and references therein].

B-type calcites from the Mont Blanc and the Aar Massifs likely result from the mixing of a shallow ^{13}C-enriched fluid derived from the Helvetic sediments and an external deep-seated ^{13}C-depleted fluid. Despite any evidence, this deep-seated fluid could partially mix with a metamorphic fluid derived from decarbonation of the metamorphic Variscan basement.

8.4. Tectonic Implications and Scale of Fluid Circulations

From the preceding discussion, the formation of Alpine veins in the Aar Massif, the MBM and its metasedimentary cover, is attributed to fluid-rock interactions with three different fluids: (1) an upper crust H_2O-CO_2-rich fluid with carbon and oxygen isotopes compositions buffered by the Helvetic metasediments, (2) a H_2O-rich fluid buffered by the Mont Blanc and the Aar crystalline rocks, and (3) a deep-seated fluid with carbon isotope composition buffered by mantle- or lower crust-derived rocks and oxygen isotope composition buffered by

the vein's immediate host rock. As these reservoirs are located at various depths in the continental lithosphere, the formation of Alpine veins in the MBM involved fluid redistribution at various scales.

Combining the $^{40}Ar/^{39}Ar$ dates with the stable isotope data in vein minerals, the following fluid flow and tectonic model is proposed:

1. Ductile deformation, related to shear zones development starting at 23–25 Ma in both the Aar and the Mont Blanc crystalline massifs. Ductile recrystallization of phengite in the shear zones goes on until 12 Ma [*Challandes et al*., 2008; *Rolland et al*., 2007, 2008, 2009].
2. Opening of the alpine veins at 16 Ma and mineral precipitation from 16 Ma to about 11 Ma, at 300–450°C. Quartz and chlorite precipitate in veins hosted in crystalline rocks, from a locally derived H_2O-rich fluid that possibly leached the vein's walls (quartz and biotite dissolution) [*Rossi et al*., 2005]. Veins hosted in the Helvetic schists probably opened at the same time as the ECM hosted veins and precipitate calcite ± quartz from a locally derived H_2O-CO_2-rich fluid. This first stage of vein filling thus occurred in a closed system. Stable isotope data suggest two stages of vein mineral precipitation (400–450°C and 300–350°C), which is consistent with $^{40}Ar/^{39}Ar$ dating of vein minerals and shear zones. Ductile shear zones were still active during alpine vein opening, so that the 16–11 Ma period represents the ductile-brittle transition.
3. The presence of calcite within veins hosted in magmatic rocks suggests later opening of the system and infiltration of an external CO_2-rich fluid. From the above discussion, the intermediate $\delta^{13}C$ values of B-type calcite indicate mixing of a deep-seated fluid with a shallower fluid derived from the Helvetic schists. Infiltration of a fluid originated from the adjacent Helvetic sediments indicate a connectivity of the Mont Blanc shear zones with the sediments, and therefore fluid flow at a several kilometer scale. In the Aar crystalline rocks, brittle faults and cataclasites are dated at 9 Ma to 3 Ma [*Kralik et al*., 1992]. Calcite precipitation in Alpine veins might thus be associated with this brittle deformation that would allow fluid flow through various crustal levels (>kilometer scale).

The isotopic composition of the fluid originating from the deep source occurred in association with major deep-seated geological features. Based on the ECORS-CROP seismic transect across the Mont Blanc area [*Tardy et al*., 1990; *Roure et al*., 1996], the MBM major shear zone can be related to steeply dipping crustal-scale shear zones and thrusts (Figure 13) that are located at the back of a crustal-scale ramp [*Leloup et al*., 2005, and references therein]. Low $\delta^{13}C$ values thus occur along crustal-scale structures that are interpreted as a transpressive pop-up system at the extremity of the Rhone dextral strike-slip system [*Marquer and Gapais*, 1985; *Marquer*, 1990; *Hubbard and Mancktelow*, 1992; *Rolland et al*., 2012]. This pop-up structure allows fluid redistribution from deep levels (mantle- or lower crust-derived fluid) in the Alpine thrust pile via active, crustal scale, and hydrologically connected shear zone networks. The fluid pathway suggested by the Alps crustal-scale geometry (Figure 13) connects down into the Penninic Front shear zone, rooting down at the base of the Internal Alps accretionary prism, which includes contrasted metamorphic ophiolitic units bounded by serpentinite-rich shear zones [e.g., *Rolland et al*., 2000]. It is thus likely that the upward fluid flow percolated through the serpentinite-rich domains. From the present example, it is thus suggested that the major shear zones provide crustal-scale fluid pathways connecting upper crust fluids to a deep-seated ascending fluid.

9. Conclusions

Using stable isotopes and $^{40}Ar/^{39}Ar$ dating, we discuss the time of fluid flow and the nature of the involved fluid reservoirs in the Alpine collisional orogeny:

1. Vein opening operated as a joint system between major shear zones that formed between 16 to 12 Ma in the Mont Blanc and the Aar Massifs. In the two massifs, adularia is shown to have grown progressively from 14–16 Ma to 9–10 Ma and mainly at 11–12 Ma. Therefore, the vein system remained open to fluid circulation during 4 to 5 Ma.
2. The $\delta^{18}O$ composition of vein minerals is generally buffered by the vein's host rock. However, the oxygen isotope composition of vein minerals allowed identification of two episodes of vein fillings: a first episode with two crystallization stages of quartz + chlorite, followed by a later episode with calcite crystallization.
3. The $\delta^{18}O$-$\delta^{13}C$ values of calcite allow identification of three end-members that can be related to different fluid chemical compositions: $\delta^{13}C_{A\text{-}type} = -4.10$ to $+3.90‰$, $\delta^{13}C_{B\text{-}type} = -6.72$ to $-2.77‰$,

and $\delta^{13}C_{C\text{-}type} = -10.75$ to -8.82‰. These compositions define a trend from the Helvetic metasedimentary schists (A-type end-member) to the core of the MBM (C-type end-member), reflecting fluid mixing through the shear zone network.

4. Veins hosted in the Mont Blanc sedimentary cover (A type) formed in an almost closed system, by interaction with a H_2O-CO_2-rich fluid derived from the Helvetic schists. A few samples show evidences of fluid mixing between this locally derived fluid and a ^{13}C-depleted fluid (C type).
5. In contrast, in the Mont Blanc crystalline massif, vein quartz and vein chlorite are not in isotopic equilibrium with calcite. Quartz and chlorite crystallized in equilibrium with a locally derived H_2O-rich fluid, whereas calcite crystallized from the infiltration of an external H_2O-CO_2-rich fluid. The $\delta^{13}C$ values of B-type veins suggest mixing of the CO_2-rich fluid derived from the Helvetic schists (A type) with a deep-seated ^{13}C-depleted fluid (C type). This deep fluid has flowed upward through vertical shear zones likely connected to the Penninic Front.
6. As for the Mont Blanc, vein calcite hosted in the Aar crystalline rocks crystallized from a fluid with a low carbon isotope composition that likely results from more efficient mixing of a H_2O-CO_2-rich fluid derived from the Helvetic schists with a deep-seated or basement-derived ^{13}C-depleted H_2O-CO_2-rich fluid.

Consequently, it is shown that prolonged episodic multiscale fluid flow occurred in the ECMs and their sedimentary cover during the Alpine orogeny: (i) fluid-rock interactions in closed systems are shown by locally derived H_2O-rich fluid and mass-balance calculations comparing veins and their host rocks within the ECMs and in the Helvetic schists, (ii) infiltration of a H_2O-CO_2-rich fluid from the Helvetic sediments in the ECMs highlights fluid migration at some several kilometer scale, and (iii) fluid-rock interaction occurred in an open system at crustal scale as shown by the infiltration of a deep-seated ^{13}C-depleted H_2O-CO_2-rich fluid along crustal-scale shear zones and thrusts in the ECMs and in their sedimentary cover.

Acknowledgments

This work was supported by INSU 3F grant to M. Rossi and Y. Rolland. The authors would like to acknowledge Kevin Faure for isotopic analyses in silicates, and H. Scott-Gagan and J, Cali (RSES) for C/O isotope analyses of calcites, while the help of S. Gallet for Ar/Ar data processing is much appreciated. The authors are grateful to S.F. Cox, N. Mancktelow, and G. Pennacchioni for support and for sharing their experience both in the lab and in the field. O. Vidal, E. Carrio, A.M. Boullier, and E. Pili are warmly acknowledged for useful discussions and support. Review from J.S. Lackey on a preliminary version and very constructive reviews of D. Marquer and T. Labotka on the submitted version were very useful and helped improve significantly the manuscript.

References

Antoine, P., J. L. Pairis, and B. Pairis (1975), Quelques observations nouvelles sur la structure de la couverture sédimentaire interne du massif du Mont Blanc, entre le Col du Ferret (frontière italo-suisse) et la Tête des Fours (Savoie, France), *Géol. Alpine*, *51*, 5–23.

Badertscher, N., R. Abart, M. Burckhard, and A. McCaig (2002), Fluid flow pathways along the Glarus overthrust derived from stable and Sr-isotope patterns, *Am. J. Sci.*, *302*, 517–547.

Baggio, P. (1958), *Il Granito del Monte Bianco e le sue Mineralizzazioni Uranifere*, vol. 1, pp. 1–130, Studi e ricerche della divisione geomineraria CNRN, Roma.

Baumgartner, L. P., and D. Rumble (1988), Transport of stable isotopes. I. Development of a kinetic continuum theory for stable isotope transport, *Contrib. Mineral. Petrol.*, *98*, 417–430.

Bellière, J. (1988), On the age of mylonites within the Mont Blanc Massif, *Geodinamica Acta*, *2*, 13–16.

Berger, A., E. Gnos, E. Janots, M. Whitehouse, M. Soom, R. Frei, and T. E. Waight (2013), Dating brittle tectonic movements with cleft monazite: Fluid-rock interaction and formation of REE-minerals, *Tectonics*, *32*, 1176–1189, doi:10.1002/tect.20071.

Berntat, W., and H. U. Bambauer (1982), The microcline/sanidine transformation isograd in metamorphic regions: II. The region of Lepontine metamorphism, central Swiss Alps, *Schweiz. Mineral. Petrogr. Mitt.*, *62*, 231–244.

Bertini, G., M. Marcucci, R. Nevini, P. Passerini, and G. Sguazzoni (1985), Patterns of faulting in the Mont Blanc granite, *Tectonophysics*, *111*, 65–106.

Bonin, B., et al. (1993), Late Variscan magmatic evolution of the Alpine basement, in *Pre-Mesozoic Geology in the Alps*, edited by J. F. von Raumer and F. Neubauer, Springer, Heidelberg.

Burkhard, M., R. Kerrich, R. Maas, and W. S. Fyfe (1992), Stable and Sr-isotope evidence for fluid advection during thrusting of the Glaurus nappe (Swiss Alps), *Contrib. Mineral. Petrol.*, *112*, 293–322.

Bussy, F. (1990), Pétrogenèse des enclaves microgrenues associées aux granitoïdes calco-alcalins: Exemple des massifs varisque du Mont Blanc (Alpes occidentales) et miocène du Monte Capanne (Ile d'Elbe, Italie), *Mémoire de Géologie de Lausanne*, *7*, 309.

Bussy, F., and J. F. von Raumer (1994), U-Pb geochronology of Palaeozoic magmatic events in the Mont Blanc crystalline Massif, Western Alps, *Schweiz. Mineral. Petrogr. Mitt.*, *74*, 514–515.

Campani, M., N. Mancktelow, D. Seward, Y. Rolland, and W. Müller (2010), Geochronological evidence for continuous exhumation through the ductile-brittle transition along a crustal-scale low-angle normal fault (Simplon Fault Zone, central Alps), *Tectonics*, *29*, TC3002, doi:10.1029/2009TC002582.

Cartigny, P., N. Jendrzejewski, F. Pineau, E. Petit, and M. Javoy (2001), Volatile (C, N, Ar) variability in MORB and the respective roles of mantle source heterogeneity and degassing: The case of the Southwest Indian Ridge, *Earth Planet. Sci. Lett.*, *194*, 241–257.

Cartwright, I., and A. C. Barnicoat (2003), Geochemical and stable isotope resetting in shear zones from Täschalp: Constraints on fluid flow during exhumation in the Western Alps, *J. Metamorph. Geol.*, *21*(2), 143–161.

Cathelineau, M., and D. Nieva (1985), A chlorite solid solution geothermometer: The Los Azufres (Mexico) geothermal system, *Contrib. Mineral. Petrol.*, *91*, 235–244.

Cenki-Tok, B., J. R. Darling, Y. Rolland, B. Dhuime, and C. G. Storey (2014), Direct dating of mid-crustal shear zones with synkinematic allanite: New in situ U-Th-Pb geochronological approaches applied to the Mont Blanc Massif, *Terra Nova*, *26*, 29–37, doi:10.1111/ter.12066.

Ceriani, S., B. Fügenschuh, and S. M. Schmid (2001), Multi-stage thrusting at the Penninic Front in the Western Alps between Mont Blanc and Pelvoux Massifs, *Int. J. Earth Sci.*, *90*, 685–702.

Chacko, T., T. K. Mayeda, R. N. Clayton, and J. R. Goldsmith (1991), Oxygen and carbon isotopic fractionation between CO_2 and calcite, *Geochim. Cosmochim. Acta*, *55*, 2867–2882.

Challandes, N. (2001), Comportement des systèmes isotopiques $^{40}Ar/^{39}Ar$ et Rb-Sr dans les zones de cisaillement: Exemples du massif de l'Aar (Massifs Cristallins Externes) et de la nappe de Suretta (Alpes Centrales Suisses), PhD University of Neuchatel, Switzerland.

Challandes, N., D. Marquer, and I. M. Villa (2008), P-T-t modelling, fluid circulation, and ^{39}Ar–^{40}Ar and Rb–Sr mica ages in the Aar Massif shear zones (Swiss Alps), *Swiss J. Geosci.*, *101*, 269–288.

Coplen, T. B., C. Kendall, and J. Hopple (1983), Comparison of stable isotope reference samples, *Nature*, *302*, 236–238.

Coward, M., and D. Dietrich (1989), Alpine tectonics—An overview, in *Alpine Tectonics*, edited by M. P. Coward, D. Dietrich, and R. G. Park, *Geol. Soc. London Spec. Publ.*, *45*, 1–29.

Crespo-Blanc, A., H. Masson, J. C. Hunziker, M. Cosca, and Z. Sharp (1995), A stable and $^{40}Ar/^{39}Ar$ isotope study of a major thrust in the Helvetic nappes (Swiss Alps) evidence for fluid flow and constraints on nappe kinematics, *J. Geol. Soc. Am. Bull.*, *107*, 1129–1144.

de Oliveira, C. G., and R. V. Santos (2003), Isotopic domains controlled by transtensional and transpressional sectors in the auriferous Diadema shear belt, northern Brazil, *J. South Am. Earth Sci.*, *16*, 513–522.

Deines, P. (2002), The carbon isotope geochemistry of mantle xenoliths, *Earth Sci. Rev.*, *58*, 247–278.

Dietrich, D., J. A. McKenzie, and H. Song (1983), Origin of calcite in syntectonic veins as determined from carbon-isotope ratios, *Geology*, *11*(9), 547–551.

Dipple, G. M., and J. M. Ferry (1992), Metasomatism and fluid flow in ductile fault zones, *Contrib. Mineral. Petrol.*, *112*, 149–164.

Duchêne, S., J. Blichert-Toft, B. Luais, P. Télouk, J.-M. Lardeaux, and F. Albarède (1997), The Lu–Hf dating of garnets and the ages of the Alpine high-pressure metamorphism, *Nature*, *387*, 586–589.

Dunn, S. R., and J. W. Valley (1992), Calcite-graphite isotope thermometry: A test for polymetamorphism in marbles, Tudor gabbro aureole, Ontario, Canada, *J. Metamorph. Geol.*, *10*, 487–501.

Escher, A., H. Masson, and A. Steck (1993), Nappe geometry in the Western Swiss Alps, *J. Struct. Geol.*, *15*, 501–509.

Fabre, C., M. C. Boiron, J. Dubessy, M. Cathelineau, and D. A. Banks (2002), Paleofluid chemistry of a single fluid event: A bulk and in-situ multi-technique analysis (LIBS, Raman Spectroscopy) of an Alpine fluid (Mont-Blanc), *Chem. Geol.*, *182*(2–4), 249–264.

Ferrando, S. (2012), Mg-metasomatism of metagranitoids from the Alps: Genesis and possible tectonic scenarios, *Terra Nova*, *24*(6), 423–436.

Ferry, J. M., and G. M. Dipple (1991), Fluid flow, mineral reactions, and metasomatism, *Geology*, *19*, 211–214.

Ferry, J. M., and M. L. Gerdes (1998), Chemically reactive fluid flow during metamorphism, *Annu. Rev. Earth Planet. Sci.*, *26*, 255–87.

Fourcade, S., D. Marquer, and M. Javoy (1989), $^{16}O/^{18}O$ variations and fluid circulation in a deep shear zone: The case of the Alpine ultramylonites from the Aar Massif (central Alps, Switzerland), *Chem. Geol.*, *77*, 119–131.

Frey, M. (1987), *Low Temperature Metamorphism*, 351 pp., Chapman and Hall, New York.

Frey, M. (1988), Discontinuous inverse metamorphic zonation, Glarus Alps, Switzerland: Evidence from illite "crystallinity" data, *Schweiz. Mineral. Petrogr. Mitt.*, *68*, 171–183.

Frey, M., and R. Mählmann Ferreiro (1999), Alpine metamorphism of the central Alps (central Alps, Alpine metamorphism, low-grade metamorphism, P-T-t path), *Schweiz. Mineral. Petrogr. Mitt.*, *79*, 135–154.

Frey, M., M. Teichmüller, R. Teichmüller, J. Mullis, B. Künzi, A. Breitschmid, U. Gruner, and B. Schwier (1980), Very low-grade metamorphism in external parts of the central Alps: Illite crystallinity, coal rank and fluid inclusion data, *Eclogae Geol. Helv.*, *73*, 173–203.

Frey, M., J. Desmons, and F. Neubauer (1999), The new metamorphic map of the Alps: Introduction, *Schweiz. Mineral. Petrogr. Mitt.*, *79*, 1–4.

Friedman, I., and J. D. Gleason (1973), A new silicate intercomparison standard for ^{18}O analysis, *Earth Planet. Sci. Lett.*, *18*(1), 124.

Gasquet, D., J.-M. Bertrand, J.-L. Paquette, J. Lehmann, G. Ratzov, R. D. A. Guedes, M. Tiepolo, A.-M. Boullier, S. Scaillet, and S. Nomade (2010), Miocene to Messinian deformation and hydrothermal activity in a pre-Alpine basement massif of the French Western Alps: New U–Th–Pb and argon ages from the Lauzière Massif, *Bull. Soc. Géol. France*, *181*, 227–241.

Glazner, A. F., and J. M. Bartley (1991), Volume loss and state of strain extensional mylonites from the central Mojave Desert, California, *J. Struct. Geol.*, *13*(5), 587–584.

Goncalves, P., E. Oliot, D. Marquer, and J. A. D. Connolly (2012), Role of chemical processes on shear zone formation: An example from the Grimsel metagranodiorite (Aar Massif, central Alps), *J. Metamorph. Geol.*, *30*(7), 703–722.

Goncalves, P., D. Marquer, E. Oliot, and C. Durand (2013), Thermodynamic modeling and thermobarometry of metasomatized rocks, in *Metasomatism and the Chemical Transformation of Rock: The Role of Fluids in Terrestrial and Extraterrestrial Processes*, *Lect. Notes Earth Syst. Sci.*, vol. 6, edited by D. E. Harlov and A. Austrheim, 800 pp., Springer, Berlin, Heidelberg.

Graham, C. M., J. Atkinson, and R. S. Harmon (1984), Hydrogen isotope fractionation in the system chlorite-water, *NERC 6th Progress Report of Research 1981–1984*, *NERC Publ. Ser. D*, vol. 25, 139 pp.

Henry, C., M. Burkhard, and B. Goffé (1996), Evolution of synmetamorphic veins and their wallrocks through a Western Alps transect: No evidence for large-scale fluid flow—Stable isotope, major-and trace element systematics, *Chem. Geol.*, *127*, 81–109.

Hillier, S., and B. Velde (1992), Chlorite interstratified with a 7Å mineral: An example from offshore Norway and possible implications for the interpretation of the composition of diagenetic chlorites, *Clay Miner.*, *27*, 475–486.

Hoefs, J. (1987), *Stable Isotope Geochemistry*, 3rd ed., Springer, Berlin.

Hoernes, S., and H. Friedrichsen (1980), Oxygen and hydrogen isotopic composition of Alpine and pre-Alpine minerals of Swiss central Alps, *Contrib. Mineral. Petrol.*, *72*, 19–32.

Horita, J. (2001), Carbon isotope exchange in the system CO_2-CH_4 at elevated temperatures, *Geochim. Cosmochim. Acta*, *65*, 1907–1919.

Hubbard, M., and N. S. Mancktelow (1992), Lateral displacement during Neogene convergence in the Western and central Alps, *Geology*, *20*, 943–946.

Hunziker, J. C., M. Frey, N. Clauer, R. D. Dallmeyer, H. Friedrichsen, W. Flehmig, K. Hochstrasser, P. Roggwiler, and H. Schwander (1986), The evolution of illite to muscovite: Mineralogical and isotopic data from Glarus Alps, Switzerland, *Contrib. Mineral. Petrol.*, *29*, 157–180.

International Atomic Energy Agency (IAEA) (1998), AQSC catalogue for reference materials and intercomparisons exercises 1998/1999, Vienna.

Javoy, M., F. Pineau, and H. Delorme (1986), Carbon and nitrogen isotopes in the mantle, *Chem. Geol.*, *57*, 41–62.

Jourdan, F., G. Féraud, H. Bertrand, A. B. Kampunzu, G. Tshoso, B. Le Gall, J. J. Tiercelin, and P. Capiez (2004), The Karoo Junction questioned: Evidence from the Jurassic and Proterozoic $^{40}Ar/^{39}Ar$ ages and geochemistry of the giant Okavango dyke swarm (Botswana), *Earth Planet. Sci. Lett.*, *222*, 989–1006.

Kerrick, R., R. D. Beckinsale, and N. J. Chackleton (1978), The physical and hydrothermal regime of tectonic vein systems: Evidence from stable isotope and fluid inclusion studies, *Neues Jahrb. Mineral. Abh.*, *131*(3), 225–239.

Kerrick, R., I. Allison, R. L. Barnett, S. Moss, and J. Starkey (1980), Microstructural and chemical transformations accompanying deformation of granite in a shear zone at Miéville, Switzerland; with applications for stress corrosion cracking and superplastic flow, *Contrib. Mineral. Petrol.*, *73*, 221–242.

Kirschner, D. L., M. A. Cosca, H. Masson, and J. C. Hunziker (1996), Staircase $^{40}Ar/^{39}Ar$ spectra of fine-grained white mica: Timing and duration of deformation and empirical constraints on argon diffusion, *Geology*, *24*, 747–750.
Kirschner, D. L., H. Masson, and Z. D. Sharp (1999), Fluid migration through thrusts faults in the Helvetic nappes (Western Swiss Alps), *Contrib. Mineral. Petrol.*, *136*, 169–183.
Kotarba, M. J., and J. L. Clayton (2003), A stable carbon isotope and biological marker study of Polish bituminous coals and carbonaceous shales, *Coal Geol.*, *55*, 73–94.
Kralik, M., N. Clauer, R. Holnsteiner, H. Huemer, and F. Kappel (1992), Recurrent fault activity in the Grimsel test site (GTS, Switzerland), revealed by Rb–Sr, K–Ar and tritium isotope techniques, *J. Geol. Soc. London*, *149*, 293–301.
Kyser, T. K. (1986), Stable isotope variations in the mantle, in *Stable Isotopes in High Temperature Geological Processes*, edited by J. W. Valley, H. P. Taylor, and J. R. O'Neil, *Rev. Mineral.*, *16*, 141–164.
Lattanzi, P., D. M. Rye, and J. M. Rice (1980), Behavior of ^{13}C and ^{18}O in carbonates during contact metamorphism of Marysville, *Am. J. Sci.*, *280*, 890–906.
Leloup, P. H., N. Arnaud, E. R. Sobel, and R. Lacassin (2005), Alpine thermal and structural evolution of the highest external crystalline massif: The Mont Blanc, *Tectonics*, *24*, TC4002, doi:10.1029/2004TC001676.
Leutwein, F., B. Poty, J. Sonet, and J. L. Zimmerman (1970), Age des cavités à cristaux du granite du Mont Blanc, *C. R. Acad. Sci. Paris*, *271*, 156–158.
Livi, K. J. T., J. M. Ferry, D. R. Veblen, M. Frey, and J. A. D. Connolly (2000), Reactions and physical conditions during metamorphism of Liassic aluminous black shales and marls in central Switzerland, *Eur. J. Mineral.*, *14*, 647–672.
Marquer, D. (1990), Structures et deformation alpine dans les granites hercyniens du massif du Gothard (Alpes centrales suisses), *Eclogae Geol. Helv.*, *83*(1), 77–97.
Marquer, D., and M. Burkhard (1992), Fluid circulation, progressive deformation and mass-transfer processes in the Upper crust: The example of basement-cover relationships in the External Crystalline Massifs, Switzerland, *J. Struct. Geol.*, *14*, 1047–1057.
Marquer, D., and D. Gapais (1985), Les massifs cristallins externes sur une transversale Guttanen-Val Bedretto (Alpes centrales): Structures et histoire cinématique, *C. R. Acad. Sci., Ser. II*, *8*, 543–546.
Marquer, D., and J. J. Peucat (1994), Rb/Sr systematics of recrystallized shear zones are the greenschist-amphibolite transition: Examples from granites in the Swiss central Alps, *Schweiz. Mineral. Petrogr. Mitt.*, *74*, 343–358.
Marquer, D., D. Gapais, and R. Capdevila (1985), Comportement chimique et orthogneissification d'une granodiorite e faciès schiste verts (Massif de l'Aar, Alpes centrales), *Bull. Mineral.*, *108*, 209–221.
Marquer, D., E. Petrucci, and P. Iacumin (1994), Fluid advection in shear zones—Evidence from geological and geochemical relationships in the Aiguilles Rouges Massif (Western Alps, Switzerland), *Schweiz. Mineral. Petrogr. Mitt.*, *74*, 137–148.
Marro, C. (1986), Les granitoïdes du Mont Blanc en Suisse, PhD thesis, Univ. of Fribourg, Switzerland.
Marshall, D., D. Kirschner, and F. Bussy (1997), A Variscan pressure-temperature-time path for the NE Mont Blanc Massif, *Contrib. Mineral. Petrol.*, *126*, 416–428.
Marshall, D., H. R. Pfeifer, J. C. Hunziker, and D. Kirschner (1998), A pressure-temperature-time path for the NE Mont Blanc Massif: Fluid-inclusion, isotopic and thermobarometric evidence, *Eur. J. Mineral.*, *10*, 1227–12,240.
McCaig, A. M., S. M. Wickham, and J. H. P. Taylor (1990), Deep fluid circulation in Alpine shear zones, Pyrenees, France: Field and oxygen isotope studies, *Contrib. Mineral. Petrol.*, *106*, 41–60.
McCrea, J. M. (1950), On the isotopic chemistry of carbonates and a paleotemperature scale, *J. Chem. Phys.*, *18*, 849–857.
Mullis, A. M. (1996), P-T-t path of quartz formation in extensional veins of the central Alps, *Schweiz. Mineral. Petrogr. Mitt.*, *76*, 159–164.
Mullis, J., J. Dubessy, B. Poty, and J. O'Neil (1994), Fluid regimes during late stages of continental collision: Physical, chemical, and stable isotope measurements of fluid inclusions quartz from a geotraverse through the central Alps, Switzerland, *Geochim. Cosmochim. Acta*, *58*, 2239–2267.
Nabelek, P. I. (1987), General equations for modelling fluid/rock interaction using trace elements, and isotopes, *Geochim. Cosmochim. Acta*, *51*, 1765–1769.
Nabelek, P. I., T. C. Labotka, J. R. O'Neil, and J. J. Papike (1984), Contrasting fluid/rock interaction between the Notch Peak granitic intrusion and argilites and limestones in the western Utah: Evidence from stable isotopes and phase assemblages, *Contrib. Mineral. Petrol.*, *86*, 25–34.
Oliver, N. H. S., and P. D. Bons (2001), Mechanisms of fluid flow and fluid-rock interaction in fossil metamorphic hydrothermal systems inferred from vein-wallrock patterns, geometry and microstructure, *Geofluids*, *1*, 137–162.
Pili, E., Y. Ricard, J. M. Lardeaux, and S. M. F. Sheppard (1997), Lithospheric shear zones and mantle-crust connections, *Tectonophysics*, *280*, 15–29.
Poty, B. (1969), La croissance des cristaux de quartz dans les filons sur l'exemple du filon de la Gardette (Bourg d'Oisans) et des filons du massif du Mont Blanc, PhD thesis, Mémoire 17, Université de Nancy.
Poty, B., H. A. Stadler, and A. M. Weisbrod (1974), Fluid inclusion studies in quartz from fissures of the Western and central Alps, *Schweiz. Mineral. Petrogr. Mitt.*, *54*, 717–752.
Raimondo, T., C. Clark, M. Hand, and K. Faure (2011), Assessing the geochemical and tectonic impacts of fluid–rock interaction in mid-crustal shear zones: A case study from the intracontinental Alice Springs Orogen, central Australia, *J. Metamorph. Geol.*, *29*, 821–850, doi:10.1111/j.1525-1314.2011.00944.x.
Richards, I. J., J. B. Connelly, R. T. Gregory, and D. R. Gray (2002), The importance of diffusion, advection, and host-rock lithology on vein formation: A stable isotope study from the Paleozoic Ouachita orogenic belt, Arkansas and Oklahoma, *Geol. Soc. Am. Bull.*, *114*(11), 1343–1355.
Rolland, Y., J.-M. Lardeaux, S. Guillot, and C. Nicollet (2000), Extension syn-convergence, poinçonnement vertical et unités métamorphiques contrastées en bordure Ouest du Grand Paradis (Alpes Franco-Italiennes), *Geodinamica Acta*, *13*, 133–148.
Rolland, Y., S. F. Cox, A. M. Boullier, G. Pennachioni, and N. Mancktelow (2003), Rare earth and trace element mobility and fractionation in mid-crustal shear zones: Insights from the Mont-Blanc Massif (Western Alps), *Earth Planet. Sci. Lett.*, *214*, 203–219.
Rolland, Y., M. Corsini, M. Rossi, S. F. Cox, G. Pennacchioni, N. Mancktelow, and A. M. Boullier (2007), Comment on "Alpine thermal and structural evolution of the highest external crystalline massif: The Mont Blanc" by P. H. Leloup, N. Arnaud, E. R. Sobel, R. Lacassin, *Tectonics*, *26*, TC2015, doi:10.1029/2006TC001956.
Rolland, Y., M. Rossi, S. F. Cox, M. Corsini, N. Mancktelow, G. Pennacchioni, M. Fornari, and A. M. Boullier (2008), $^{40}Ar/^{39}Ar$ dating of syn-kinematic white mica: Insights from fluid-rock reaction in low-grade shear zones (Mont Blanc Massif) and constraints on timing of deformation in the NW External Alps, in *The Internal Structure of Fault Zones: Implications for Mechanical and Fluid-Flow Properties*, edited by C. A. J. Wibberley, et al., *Geol. Soc. London Spec. Publ.*, 299, 293–315, doi:10.1144/SP299.17.
Rolland, Y., S. F. Cox, and M. Corsini (2009), Constraining deformation stages in brittle-ductile shear zones from combined field mapping and $^{40}Ar/^{39}Ar$ dating: The structural evolution of the Grimsel Pass area (Aar Massif, Swiss Alps), *J. Struct. Geol.*, *31*, 1377–1394, doi:10.1016/j.jsg.2009.08.003.

Rolland, Y., J.-M. Lardeaux, and L. Jolivet (2012), Deciphering orogenic evolution, *J. Geodyn.*, *56–57*, 1–6, doi:10.1016/j.jog.2011.09.004.
Rollinson, H. (1993), *Using Geochemical Data: Evaluation, Presentation, Interpretation*, Prentice Hall, Harlow.
Rossi, M. (2005), Déformation, transferts de matière et de fluide dans la croûte continentale: Application aux massifs cristallins externes des Alpes, PhD thesis, Univ. of Grenoble, France.
Rossi, M., Y. Rolland, O. Vidal, and S. F. Cox (2005), Geochemical variations and element transfer during shear-zone development and related épisyénites at middle crust depths: Insights from the Mont Blanc granite (French-Italian Alps), in *High Strain Zones: Structure and Physical Properties*, edited by D. Bruhn and L. Burlini, *Geol. Soc. London Spec. Publ.*, *245*, 373–396.
Roure, F., P. Choukroune, and R. Polino (1996), Deep seismic reflection data and new insights on the bulk geometry of mountain ranges, *C. R. Acad. Sci.*, *322*, 345–359.
Rowley, D. B., R. T. Pierrehumbert, and B. S. Currie (2001), A new approach to stable isotope-based paleoaltimetry: Implications for paleoaltimetry and paleohypsometry of the High Himalaya since the late Miocene, *Earth Planet. Sci. Lett.*, *188*, 253–268.
Rubatto, D., D. Gebauer, and R. Compagnoni (1999), Dating of eclogite-facies zircons: The age of Alpine metamorphism in the Sesia–Lanzo Zone (Western Alps), *Earth Planet. Sci. Lett.*, *167*, 141–158.
Sanchez, G., Y. Rolland, J. Schneider, M. Corsini, E. Oliot, P. Goncalves, C. Verati, J. M. Lardeaux, and D. Marquer (2011), Dating low-temperature deformation by $^{40}Ar/^{39}Ar$ on white mica, insights from the Argentera-Mercantour Massif (SW Alps), *Lithos*, *125*(1–2), 521–536.
Schmid, S. M., and E. Kissling (2000), The arc of the Western Alps in the light of geophysical data on deep crustal structure, *Tectonics*, *19*(1), 62–85, doi:10.1029/1999TC900057.
Sharp, Z. D. (1990), Laser-based microanalytical method for the in situ determination of oxygen isotope ratios of silicates and oxides, *Geochim. Cosmochim. Acta*, *54*, 1353–1357.
Sharp, Z. D., H. Masson, and R. Lucchini (2005), Stable isotope geochemistry and formation mechanisms of quartz veins; extreme paleoaltitude of the central Alps in the Neogene, *Am. J. Sci.*, *305*, 187–219.
Sheppard, S. M. F. (1986), Characterization and isotopic variations in natural waters, in *Stable Isotopes in High Temperature Processes*, edited by J. W. Valley, H. P. Taylor, and J. R. O'Neil, *Rev. Mineral.*, *16*, 165–183.
Simon-Labric, T., Y. Rolland, T. Dumont, T. Heymes, C. Authemayou, M. Corsini, and M. Fornari (2009), $^{40}Ar/^{39}Ar$ dating of Penninic Front tectonic displacement (W Alps) during the lower Oligocene (31–34 Ma), *Terra Nova*, *21*, 127–136.
Steck, A. (1976), Albit-oligoklas-mineralgesellschaften der peristeritluecke aus alpinmetamorphen granitgneisen des gotthardmassivs, *Schweiz. Mineral. Petrogr. Mitt.*, *56*, 269–292.
Steck, A., and G. Burri (1971), Chemismus und paragenesen von granaten aus granitgneisen der grünschiefer- und amphibolitfazies der zentralalpen, *Schweiz. Mineral. Petrogr. Mitt.*, *51*, 534–538.
Steiger, R. H., and E. Jäger (1977), Subcomission on geochronology: Convention of the use of decay constants in geo- and cosmochronology, *Earth Planet. Sci. Lett.*, *36*, 359–362.
Streit, J. E., and S. F. Cox (1998), Fluid infiltration and volume-change during mid-crustal mylonitization of Proterozoic granite, King Island, Tasmania, *J. Metamorph. Geol.*, *16*, 197–212.
Tardy, M., E. Deville, S. Fudral, S. Guellec, G. Ménard, F. Thouvenot, and P. Vialon (1990), Interprétation structurale des données du profil sismique réflexion profonde ECORS-CROP Alpes entre le front Pennique et la ligne du Canavèse (Alpes Occidentales), *Mem. Soc. Geol. Fr.*, *156*, 217–226.
Taylor, H. P., Jr. (1968), The oxygen isotope geochemistry of igneous rocks, *Contrib. Mineral. Petrol.*, *19*, 1–71.
Taylor, H. P., Jr. (1977), Water/rock interaction and the origin of H_2O in granitic batholiths, *J. Geol. Soc. London*, *133*, 509–558.
Turner, G., J. C. Huneke, F. A. Podose, and G. J. Wasserburg (1971), $^{40}Ar/^{39}Ar$ ages and cosmic ray exposure ages of Apollo 14 samples, *Earth Planet. Sci. Lett.*, *12*, 15–19.
Valley, J. W. (1986), Stable isotope geochemistry of metamorphic rocks, in *Stable Isotopes in High Temperature Geological Processes*, edited by J. W. Taylor, J. H. P. Taylor, and J. R. O'Neil, *Rev. Mineral.*, *16*, 141–164.
Valley, J. W., and D. Cole (2001), Stable isotope geochemistry, *Mineral Soc. Am. Rev. Mineral. Geochem.*, *43*, 662.
Valley, J. W., N. Kitchen, M. J. Kohn, C. R. Niendorf, and M. J. Spicuzza (1995), UWG-2, a garnet standard for oxygen isotope ratios: Strategies for high precision and accuracy with laser heating, *Geochim. Cosmochim. Acta*, *59*, 5223–5231.
Vennemann, T. W., and J. R. O'Neil (1993), A simple and inexpensive method of hydrogen isotope and water analyses of minerals and rocks based on zinc reagent, *Chem. Geol.*, *103*, 227–234.
Vidal, O., T. Parra, and F. Trotet (2001), A thermodynamic model for Fe-Mg aluminous chlorite using data from phase equilibrium experiments and natural pelitic assemblages in the 100–600°C, 1–25 kbar P-T range, *Am. J. Sci.*, *301*, 557–592.
Wenner, D. B., and H. P. Taylor Jr. (1971), Temperatures of serpentinization of ultramafic rocks based on $^{18}O/^{16}O$ fractionation between coexisting serpentine and magnetite, *Contrib. Mineral. Petrol.*, *32*, 165–185.
Zheng, Y. F. (1993), Calculation of oxygen isotope fractionation in hydroxyl-bearing silicates, *Earth Planet. Sci. Lett.*, *121*, 247–263.
Zheng, Y. F. (1999), Oxygen isotope fractionation in carbonate and sulfate minerals, *Geochem. J.*, *33*, 109–126.
Zimmermann, J. L., and B. Poty (1970), Etude par spectroscopie de masse de la composition des fluids dans les cavités alpines du massif du Mont Blanc, *Bull. Suisse Mineral. Petrogr.*, *50*(1), 99–108.